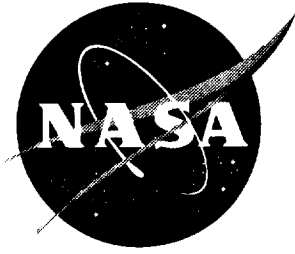NASA/CR-2000-210111

Examination of the Lateral Attenuation of Aircraft Noise

Kenneth J. Plotkin, Christopher M. Hobbs, and Kevin A. Bradley
Wyle Laboratories, Arlington, Virginia

April 2000

The NASA STI Program Office ... in Profile

Since its founding, NASA has been dedicated to the advancement of aeronautics and space science. The NASA Scientific and Technical Information (STI) Program Office plays a key part in helping NASA maintain this important role.

The NASA STI Program Office is operated by Langley Research Center, the lead center for NASA's scientific and technical information. The NASA STI Program Office provides access to the NASA STI Database, the largest collection of aeronautical and space science STI in the world. The Program Office is also NASA's institutional mechanism for disseminating the results of its research and development activities. These results are published by NASA in the NASA STI Report Series, which includes the following report types:
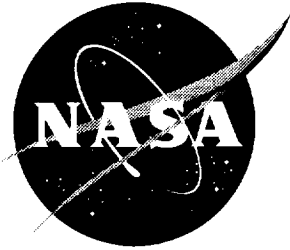
- TECHNICAL PUBLICATION. Reports of completed research or a major significant phase of research that present the results of NASA programs and include extensive data or theoretical analysis. Includes compilations of significant scientific and technical data and information deemed to be of continuing reference value. NASA counterpart of peer-reviewed formal professional papers, but having less stringent limitations on manuscript length and extent of graphic presentations.

- TECHNICAL MEMORANDUM. Scientific and technical findings that are preliminary or of specialized interest, e.g., quick release reports, working papers, and bibliographies that contain minimal annotation. Does not contain extensive analysis.

- CONTRACTOR REPORT. Scientific and technical findings by NASA-sponsored contractors and grantees.

- CONFERENCE PUBLICATION. Collected papers from scientific and technical conferences, symposia, seminars, or other meetings sponsored or co-sponsored by NASA.

- SPECIAL PUBLICATION. Scientific, technical, or historical information from NASA programs, projects, and missions, often concerned with subjects having substantial public interest.

- TECHNICAL TRANSLATION. English-language translations of foreign scientific and technical material pertinent to NASA's mission.

Specialized services that complement the STI Program Office's diverse offerings include creating custom thesauri, building customized databases, organizing and publishing research results ... even providing videos.

For more information about the NASA STI Program Office, see the following:

- Access the NASA STI Program Home Page at *http://www.sti.nasa.gov*

- E-mail your question via the Internet to help@sti.nasa.gov

- Fax your question to the NASA STI Help Desk at (301) 621-0134

- Phone the NASA STI Help Desk at (301) 621-0390

- Write to:
  NASA STI Help Desk
  NASA Center for AeroSpace Information
  7121 Standard Drive
  Hanover, MD 21076-1320

NASA/CR-2000-210111

Examination of the Lateral Attenuation of Aircraft Noise

Kenneth J. Plotkin, Christopher M. Hobbs, and Kevin A. Bradley
Wyle Laboratories, Arlington, Virginia

April 2000

Table of Contents

List of Figures

List of Figures (Continued)

List of Tables

1.0 Introduction

An important component of aircraft noise modeling is lateral attenuation: reduction of sound by the ground at shallow incidence angles. The two major noise models in use in the United States, the Federal Aviation Administration's Integrated Noise Model (INM)[1] and the Department of Defense's NOISEMAP (NMAP)[2] use empirical fits to A-weighted levels measured in flight tests. Both models consider lateral attenuation to be a function of source elevation angle, with INM also including a distance effect. The INM procedure, defined by SAE 1751[3], represents both ground effect and shielding, with shielding being noise directivity about the roll axis. The NMAP procedure represents only ground effect, with the data on which it is based having shown no significant differences between various aircraft types[4].

The two models differ from each other. They also differ from excess ground attenuation calculations based on modern ray-tracing ground impedance theory, denoted in this report as EGA theory. Figure 1 shows the SAE and NMAP models, together with a model by the Danish Acoustical Institute (DAI)[5] based on EGA theory[6]. The EGA model (which does not include refraction) depends on distance and receiver height as well as angle. Figure 1 shows the comparison for two distances, 1000 and 2000 feet, and receiver height of four feet. In addition to the SAE and NMAP models and the DAI model, Figure 1 shows a direct calculation from EGA theory[6] using a nominal spectrum similar to that used in Reference 5.

Note that the SAE model generally predicts attenuation greater than or (at small angles) comparable to the NMAP model, while ray theory is smaller than both, except at near-grazing angles.

There are two important considerations. The first is the accuracy of the current simple models, purely from a physical modeling perspective. The second is whether any inaccuracies are significant when applied to real aircraft operations, where noise sources are extended and many other non-ideal factors are involved.
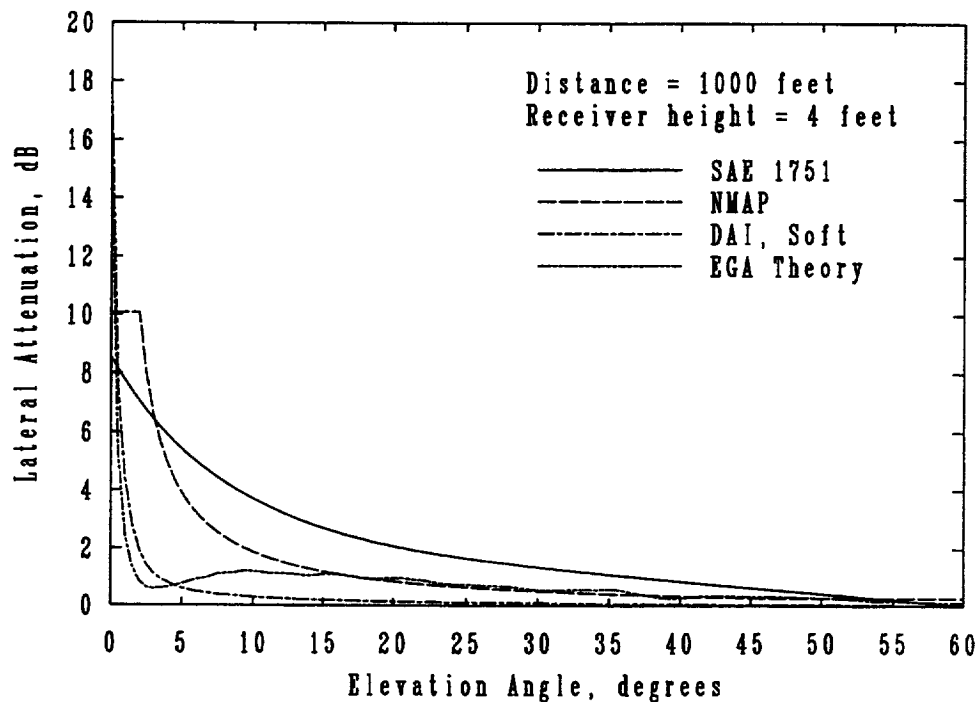
a. Distance = 1000 feet
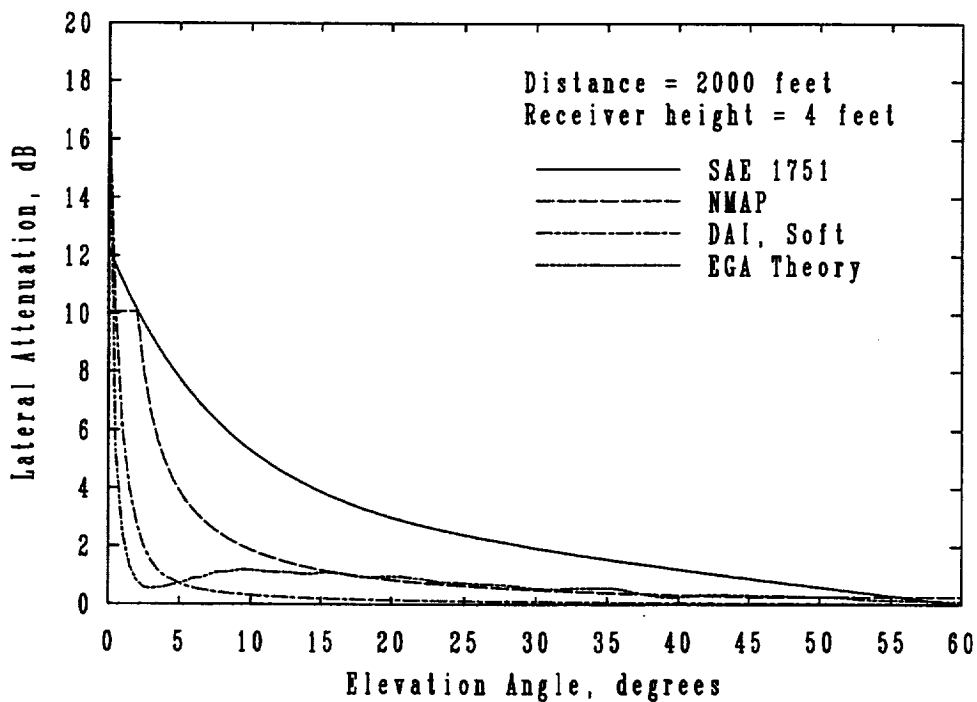
b. Distance = 2000 feet

Figure 1. Comparison of Four Lateral Attenuation Models

A measurement program was conducted to obtain sideline noise from normal operations at an airport. These measurements were conducted at Denver International Airport (DIA), in an open area north of Runway 08, and concentrated on takeoffs where elevation angles to the microphones were between zero and 30 degrees. Aircraft positions were determined by a video system. Meteorological data were collected at the site via a 10-meter tower.

Section 2 of this report presents a brief review of ground effect and lateral attenuation. Sections 3 and 4 describe the measurement program and data reduction procedures. Section 5 presents the results of the analysis.

2.0 Lateral Attenuation Theory

2.1 Modeling of Aircraft Noise

Noise from a point source above a flat ground is given by:

$$L = L_{ref} + 20 \log_{10} (r/r_{ref}) - \alpha r + A_e \tag{1}$$

where

L = sound level at receiver a distance r from the source

L_{ref} = free field sound level at a reference distance r_{ref}, with no atmospheric loss

α = atmospheric absorption coefficient, dB per unit distance

A_e = attenuation or amplification due to the ground

Both α and A_e are functions of frequency. α also depends on atmospheric conditions, and A_e (as will be elaborated shortly) depends on ground properties and source to receiver geometry.

A_e is written here as a ground effect, which is added to the sound. When A_e is positive it is an amplification, and when negative it is a loss. There is a distinction between A_e and common usage of "excess ground attenuation" and the aircraft noise modeling term "lateral attenuation". Excess ground attenuation often means the difference between the sound L at the receiver over the current ground surface and a hard surface, or sometimes the difference between L and the sound at an equivalent distance but with the receiver directly under the source, (i.e., normal incidence). The reference level L_{ref} in the definition of excess ground attenuation is not free field, but includes a reference ground effect.

Lateral attenuation in aircraft noise modeling is generally a combination of the second definition above (L_{ref} includes ground effect at normal incidence) and directivity (if any) about the aircraft's roll axis.

Both excess ground attenuation and lateral attenuation are presented as positive values to be subtracted, rather than the additive form of ground effect in Equation (1). Denoting lateral attenuation by Λ, lateral attenuation is related to ground effect by:

$$\Lambda = A_e(ref) - A_e \tag{2}$$

where (ref) refers to the reference condition of normal incidence.

Equation (1) is for a point source. INM and NMAP are line source models, where the basic noise source is a line developed from the integration of Equation (1). The noise level for the line integral of Equation (1) is the Sound Exposure Level (SEL) rather than the instantaneous sound level.

If the noise source were a monopole moving at constant speed, the SEL result would be very similar to Equation (1). In the second and third terms, radius r would be replaced with normal distance d, and the second term (log of distance) would have a factor of 10 instead of 20. There would be some relatively simple factors associated with the cumulative effects of integrating the second and third terms. The ground effect term would generally be complicated, although for the power law approximation used in highway noise modeling[7] that term also emerges with a simple point-to-line factor.

In practice, however, integration of Equation (1) for aircraft is not simple. Aircraft have significant directional patterns, with spectrum as well as amplitude varying. Atmospheric attenuation at high frequencies is substantial, and changes to spectral shape have nonlinear implications. Consequently, noise databases - the "NPD" curves in INM and the "SEL deck" part of NMAP runs – are based on direct measurements of SEL at some distance. Extrapolation of SEL to other distances is then accomplished by one of several methods defined by SAE 1845[8]. These methods are based on numerical processing of flight test data.

Because of the semi-empirical nature of the line source models, versus the formal theory for point sources, analysis of ground effect in this study concentrated on point source propagation when the aircraft was in line with a measurement array perpendicular to the runway. Application to line sources can then be accomplished by methods similar to those described in Reference 8.

2.2 Current Models

SAE 1751 defines lateral attenuation in two parts. Based on the work of Parkin and Scholes[9,10], overground propagation of a line source on the ground is given by:

$$G(d) = 15.09\left(1 - e^{-.00274d}\right)dB \ , \quad d \leq 914m \tag{3a}$$

$$G(d) = 13.86dB \qquad , \quad d > 914m \tag{3b}$$

where d is the perpendicular distance from the line to the receiver, in meters, and G is the overground lateral attenuation.

For sources above the ground and distances greater than 914 meters (3000 feet), SAE defines the following air-to-ground lateral attenuation Λ:

$$\Lambda(\beta) = 3.96 - 0.066\beta + 9.90e^{-0.13\beta}dB \ , \quad 0^{\circ} \leq \beta \leq 60^{\circ} \tag{4a}$$

$$\Lambda(\beta) = 0dB \ , \qquad\qquad\qquad 60^{\circ} < \beta \leq 90^{\circ} \tag{4b}$$

where β is the elevation angle, in degrees.

For sources above the ground and less than 914 meters from the receiver, the following transition equation is used:

$$\Lambda(\beta,d) = \frac{G(d)\Lambda(\beta)}{13.86}dB \tag{5}$$

Equation (5) reduces to (3) for zero elevation angle, and to (4) for distance greater than 914 meters. The relations are considered to include ground effects, atmospheric refraction, and aircraft shielding[11]. Note that Λ (β, d) is distinct from Λ (β).

NMAP's lateral attenuation model is based on measurements from a series of constant altitude flight tests. The following air-to-ground lateral attenuation is used:

$$\Lambda(\beta) = \left(-18.18 + 20.49/\beta\right)dB \ , \quad 2^{\circ} \leq \beta \leq 45^{\circ} \tag{6a}$$

$$\Lambda(\beta) = 10.06dB \ , \qquad\qquad 0^{\circ} \leq \beta < 2^{\circ} \tag{6b}$$

$$\Lambda(\beta) = 0.0dB \ , \qquad\qquad\quad 45^{\circ} < \beta \tag{6c}$$

Reference 4 specifies that Equation (6a) be used down to 1 degree. The 2-degree limit is current practice[13]. There is no distinct overground lateral attenuation model, but Λ (0) serves that purpose.

The two models differ from each other. Speakman[12] notes that this may be because of spectral differences between military and civil aircraft. SAE lateral attenuation includes shielding, although the single formula is used for all aircraft types. In the measurements

leading to Equations (6), no correlation was found between lateral attenuation and different aircraft types. Those measurements included single engine fighters for which no shielding would be expected and large multi-engine bombers and transports for which shielding effects could be expected. The possibility of shielding was a consideration in interpretation of the current data.

2.3 Theory for Ground Effect

Ground effect theory has been developed by a number of researchers over a considerable period of time. Reference 6, cited earlier, is a commonly cited formulation, and was used in development of the simple model of Reference 5. References 14 and 15 present equivalent theory, in a broader context of atmospheric propagation. Reference 16 is another good source for the theory, and includes procedures for predicting ground effect over finite bands (versus pure tones) and for the effect of turbulence-induced phase fluctuations on ground effect. In this study, the formulation of Reference 16 for ground effect is followed, including the band result applied to one-third octaves, but not including turbulence effects. References 6 and 14-16 cite earlier work, which has led to current theory.

Ground effect arises from the interaction between direct and reflected rays, as illustrated in Figure 2. Sound at the receiver consists of the direct ray which has traveled a distance r_1 and the reflected ray which has traveled a distance r_2 and which has experienced phase and amplitude changes at the reflection point. The reflected wave is treated as if it came from the image illustrated in Figure 2. If the ground is considered to be locally reacting (sound does not propagate within it), the reflection coefficient of a plane wave at incident angle φ is given by:

$$R_p = \frac{\sin\varphi - Z_1/Z_2}{\sin\varphi + Z_1/Z_2}$$

(7)

where Z_1 and Z_2 are the impedances of air and the ground, respectively, and the image source strength is R_p times the original source strength.
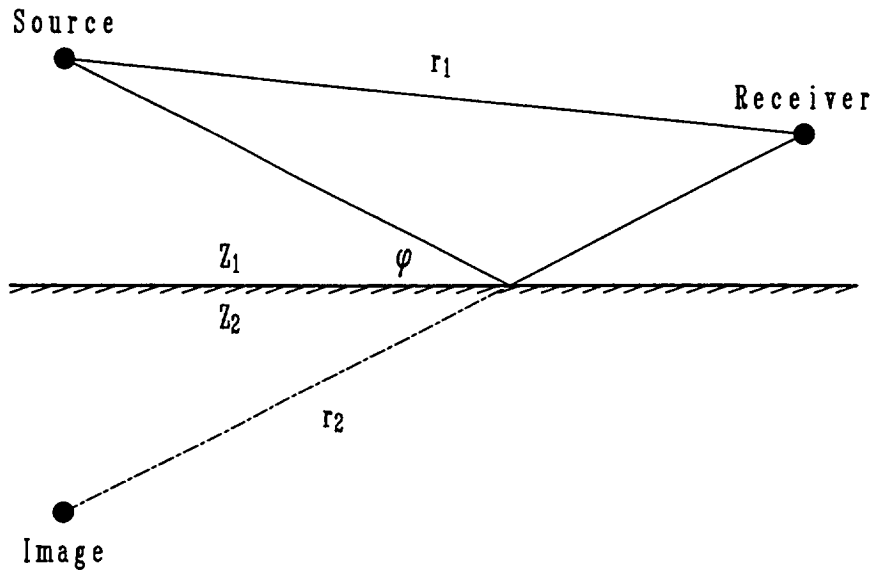
Figure 2. Geometry of Source, Receiver, Image Source and Ray Paths

The situation of interest is propagation of a spherical wave. The image source strength for a spherical wave is given by:

$$Q = R_p + F(w)(1 - R_p) \qquad (8)$$

where $F(w)$ is the boundary loss factor, and its argument w is the numerical distance. For a locally reacting ground, the numerical distance is

$$w = \tfrac{1}{2}ikr_2 \frac{(\sin\varphi + Z_1/Z_2)^2}{(1 + \sin\varphi \cdot Z_1/Z_2)} \qquad (9)$$

where k is the wave number in air. The references cited define $F(w)$, and provide practical methods for computing it.

When adding the direct and image waves, the image strength is divided by the ratio $r' = r_1/r_2$, which accounts for the amplitude difference associated with the different propagation distances. The reflected wave also has a phase shift associated with $\Delta r = r_2 - r_1$, in addition to any phase shift associated with the reflection. Expressing Q as $|Q|e^{i\theta}$, the final result for the ground effect is

$$A_e = 10 \log_{10} \left[1 + \frac{1}{r'^2} |Q|^2 + \frac{2}{r'} |Q| \cos\left(\frac{2\pi\Delta r}{\lambda} + \theta \right) \right] \tag{10}$$

where λ is the wavelength. Equation (10) is for pure tones. For a finite band of white noise, the corresponding result[16] is

$$A_e = 10 \log_{10} \left[1 + \frac{1}{r'^2} |Q_i|^2 + \frac{2}{r'} |Q_i| \sin\left(\frac{\mu\Delta r}{\lambda_i} \right) \cdot \frac{\cos\left(\eta\Delta r / \lambda_i + \theta_i \right)}{\mu\Delta r / \lambda_i} \right] \tag{11}$$

where

$$\Delta f = bandwidth$$

$$\mu = 2\pi\Delta f / 2f_i$$

$$\eta = 2\pi \left[1 + \left(\Delta f / 2f_i \right)^2 \right]^{\frac{1}{2}}$$

and $(\ )_i$ denotes that the value is to be taken at the center of the band.

Delaney and Bazley[17] showed that the impedance of a porous surface can be represented by simple polynomials that depend on the flow resistivity, σ, of the material. If

$$Z_2 = R + iX \tag{12a}$$

$$k = \alpha + i\beta \tag{12b}$$

then

$$R / \rho_0 c_0 = 1 + 9.08 \left(f / \sigma \right)^{-0.75} \tag{13a}$$

$$X / \rho_0 c_0 = -11.9 \left(f / \sigma \right)^{-0.73} \tag{13b}$$

$$\alpha / \left(\omega / c_0 \right) = 1 + 10.8 \left(f / \sigma \right)^{-0.70} \tag{13c}$$

$$\beta / \left(\omega / c_0 \right) = 10.3 \left(f / \sigma \right)^{-0.59} \tag{13d}$$

where c_0 is the speed of sound in air, $\omega = 2\pi f$, and $\rho_0 c_0$ is the impedance of air, Z_1.

The various models require slightly different parameters. The NMAP model, Equation (3), depends only on elevation angle. The SAE model, Equations (3) through (5), also requires distance. The simplified method of Reference 5 is slightly more complex than the SAE model, requiring elevation angles for both the source and receiver. It also requires a categorical variable for surface, either soft or hard.

The full EGA theory requires more parameters. The geometric parameters in the primary formulae, Equations (10) and (11), can be computed from distance between source and receiver and the source and receiver heights. The frequency [and bandwidth if Equation (11) is used] is required, as is the ground impedance. Ground impedance, as computed per Equations (12) and (13), requires one primary parameter: the flow resistance. Density and sound speed of air are also required, but these are not strong variables. The increased effort associated with EGA theory is due to computational requirements: spectral calculations are needed, and the relations are inherently more complicated.

3.0 Measurement Program

3.1 Objectives

The objective of the measurement program was to collect noise data from in-use commercial aircraft at a major air-carrier airport. Emphasis was on studying ground effect under real-world conditions. Elevation angles below about 30 degrees, and especially below 10 degrees, were therefore required. Measurements were to be tape recorded, so that spectral analysis could be performed. An initial objective was to conduct measurements for both takeoff and landing. Measurement of both would, however, have required two microphone arrays and was also problematical because the lower noise levels on approach would lead to signal-to-noise difficulties. Because spectral analysis was planned, it was decided that the effort should be limited to takeoffs only.

The basic measurements were to consist of an array of microphones at several heights and distances, deployed perpendicular to a runway. This array would be located at a position where elevation angles would be up to 30 degrees, and configured for a range of path length differences [Δr in Equations (10) and (11)] commensurate with typical aircraft noise spectra. These requirements led to a nominal design of three heights (0, 4 and 12 feet above the ground) and four to five positions evenly spaced out to a distance of 2000 to 3000 feet from the runway. This array would be deployed at a location where aircraft would be from zero to 500 feet above the runway.

A reference microphone position directly under the aircraft was desired, for a normal incidence measurement as discussed in Section 2.1. This reference position had to be located further along the flight track, beyond the end of the runway. Ideally, this would still be at a position before noise abatement cutbacks took place, so that power would be the same as when the aircraft passed the main array.

This plan required a flat area next to a runway with a significant number of departures. The following supporting requirements were noted:

1. Tape recording of aircraft noise, so that data could be processed into one-third octave bands at short (one-quarter- to one-half-second) time intervals.

2. A method to accurately track aircraft position. While ARTS radar would be available, this provides horizontal resolution of about one-eighth of a mile and vertical resolution of 100 feet, which was considered to be of insufficient accuracy. Accordingly, it was decided to use a video system to record aircraft position.

3. Access to flight records so that actual aircraft types would be known.

4. Access to local weather data.

5. Time correlation between noise and position data

3.2 Measurement Site

A site on the north side of Runway 08 at DIA was found to satisfy the above requirements. DIA was chosen on the following basis:

- coordination with general model validation studies[18]

- cooperation with the airport to obtain ARTS radar tracking and flight records

- cooperation of two major air carriers, which provided actual aircraft types and takeoff weights

- availability of a clear, flat area next to one runway and away from other activities

Figure 3 is a sketch of the runways at DIA. Runway 08-26, the east-west runway in the northeast corner of the airport, was selected. Approximately 30 percent of departures are eastward from this runway (Runway 08), including virtually all departures of Stage 2 aircraft. Stage 2 aircraft were considered to be helpful because they provide higher noise levels (and hence better signal-to-noise ratio) than Stage 3.

Runway 08-26 is 12,000 feet long, and is oriented very nearly true geographic east-west. Analysis of several sample days of ARTS radar data indicated that aircraft typically rotate between 5000 and 7000 feet from threshold. At a distance of 8000 feet from threshold aircraft would be well distributed between zero and 500 feet above the ground. This would yield elevation angles of up to 14 degrees for measurements 2000 feet to the side of the runway, and up to 45 degrees for measurements 500 feet to the side.
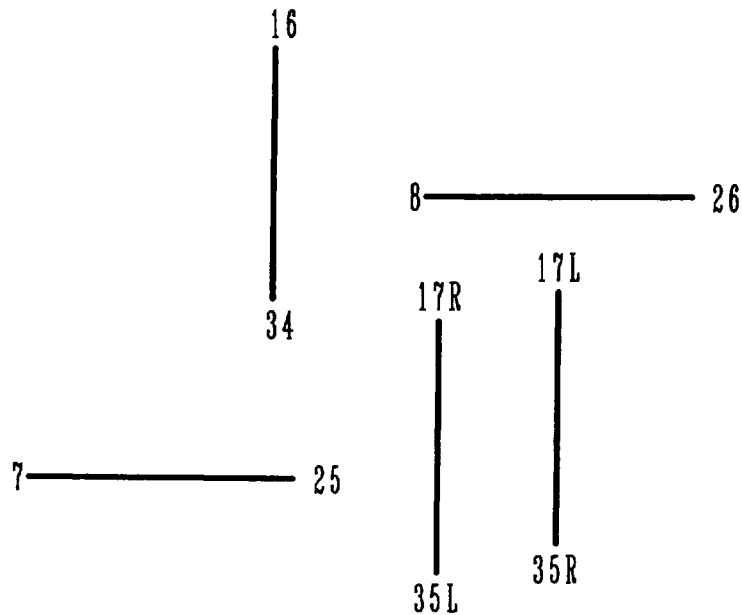
Figure 3. Runway Arrangement at Denver International Airport

Figure 4 is a plan view of the site, including the final microphone locations. Access to the area was via public roads, with Road 104 parallel to the runway and approximately one-half mile north of it. A fence is parallel to the runway, 650 feet north of it. The land north of the fence (outside of the restricted access area of the airport itself) is owned by the airport and is leased to farmers for wheat crops. Hayesmont Mile Road is north-south, and ends at a gate in the fence at a position 6150 feet east of the Runway 08 threshold. The obvious area for the microphone array is to the east of Hayesmont Mile Road, north of the fence and south of Road 104.

This area is flat from Hayesmont Mile Road eastward for a distance of approximately 1500 feet. The terrain then has a sharp drop to a slightly lower area with small hills. This uneven terrain begins about 7500 feet from threshold, and precluded use of the ideal location noted in Section 3.1. With this constraint, a position 6750 feet east of the Runway 08 threshold (600 feet east of Hayesmont Mile Road) was chosen. In the north-south extent of the flat area, there is an east-west ravine with its southern rim about 2100 feet from the center of the runway and its northern rim about 50 feet south of Road 104. The area south of the ravine allowed room for four microphone positions, nominally at 500-foot intervals from the runway centerline. Because of the fence at 650 feet, the closest microphones were placed 666 feet from the runway. The other three microphone

positions were 1000, 1500 and 2000 feet from the runway. A position on Road 104, in line with the microphone array, was chosen for the video camera.

For the reference microphone, a position was found 3400 feet east of the eastern end of the runway (15,400 feet from Runway 08 threshold), just beyond the fenced area around the runway. Access to this "end of runway" location was via a perimeter road.

Figure 4 shows the locations of the main microphone array, and the end of runway position. Figure 5 is a photograph of the site, as viewed from the camera position. Microphones and video reference targets (Section 3.4) are deployed, but are not visible in this reduced-size photograph.
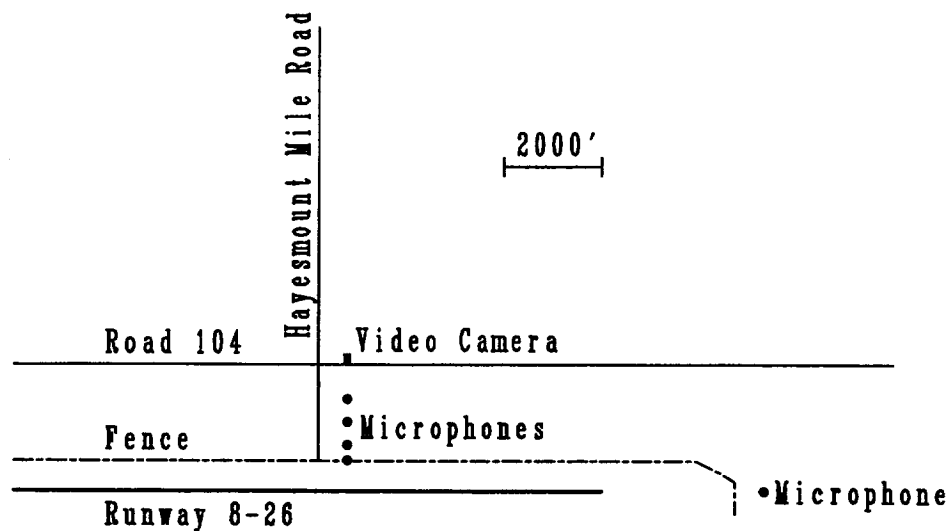
Figure 4. Layout of Measurement Site

Figure 5. Measurement Area, Looking toward Runway, Video Camera in Foreground

Figure 6 shows a cross-section of the site, with microphone positions marked. The site was not perfectly flat. The 1000 foot position was at the crest of a gentle hill, with the slope from there to the 2000 foot position being constant but about one degree different from that from the 1000 foot position to the 666 foot position. This slight difference in slope was accounted for in the analysis. The plane of the ground between the 1000- and 2000-foot positions was directly in line with the height of the runway. For analysis of noise at microphones at 1500 and 2000 feet, source height was taken to be equal to the height of the aircraft above the ground. The plane of the ground closer than 1000 feet projected to a height 17 feet below the runway surface at the runway distance. For analysis of noise at microphones at 666 and 1000 feet, the source height was taken to be the aircraft height above the runway plus 17 feet.

3.3 Acoustic Instrumentation

Acoustic instrumentation was provided by NASA in the form of two digital acoustic vans. Each van had capability of deploying up to 10 microphones, at distances of up to 3000 feet from the van.

Microphones in this instrumentation system consisted of one-half inch Bruel and Kjaer condenser microphones, with 16-bit digitizers located at each microphone. Data were digitized at a rate of 20,000 samples per second and transmitted by cable to the van. Within the van, microphone signals were converted to analog for observation of quality, then resampled and multiplexed. The multiplexed signals were recorded on 8-mm helical scan tapes. Time of day, run numbers and system gain values were also multiplexed onto tape. Time of day was derived from a GPS time code receiver, to an accuracy of one millisecond. The instrumentation systems were custom built for NASA. The tape drives were standard SCSI devices, and the tapes can be read by any computer system with a compatible interface.

Twelve microphones were deployed, at heights of zero, four, and 12 feet above the ground, and at distances of 666, 1000, 1500 and 2000 feet from the runway centerline. Six microphones were deployed from each van: the 666 and 1000 foot positions from one van, and the 1500 and 2000 foot positions from the other.

Figure 6 indicates the identification numbers of the microphones at each distance. At each distance, microphone numbers were sequential from highest to lowest, (i.e., microphones 1, 4, 7 and 10 were twelve feet high; 2, 5, 8 and 11 four feet high; and 3, 6, 9 and 12 on the ground). The 4- and 12-foot high microphones were mounted on small towers.

Figure 7 shows one of the microphone towers. Figure 8 shows placement of one of the ground microphones. Note that no ground board was employed: the objective was to measure ground effect.
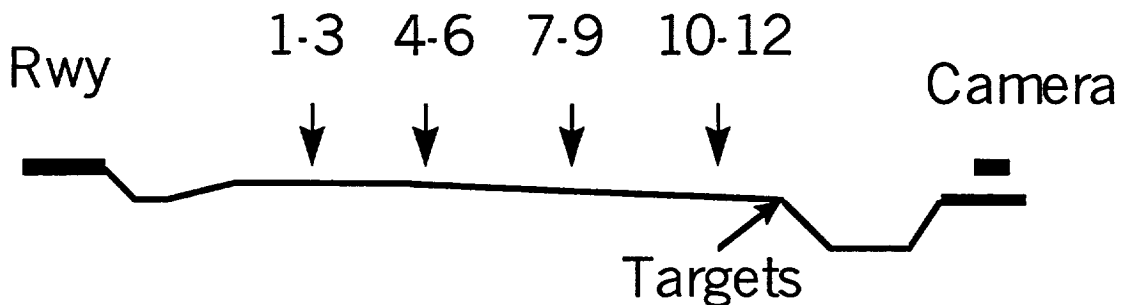
Figure 6. Cross-section of Primary Microphone Array
Microphones 666, 1000, 1500 and 2000 Feet from Runway
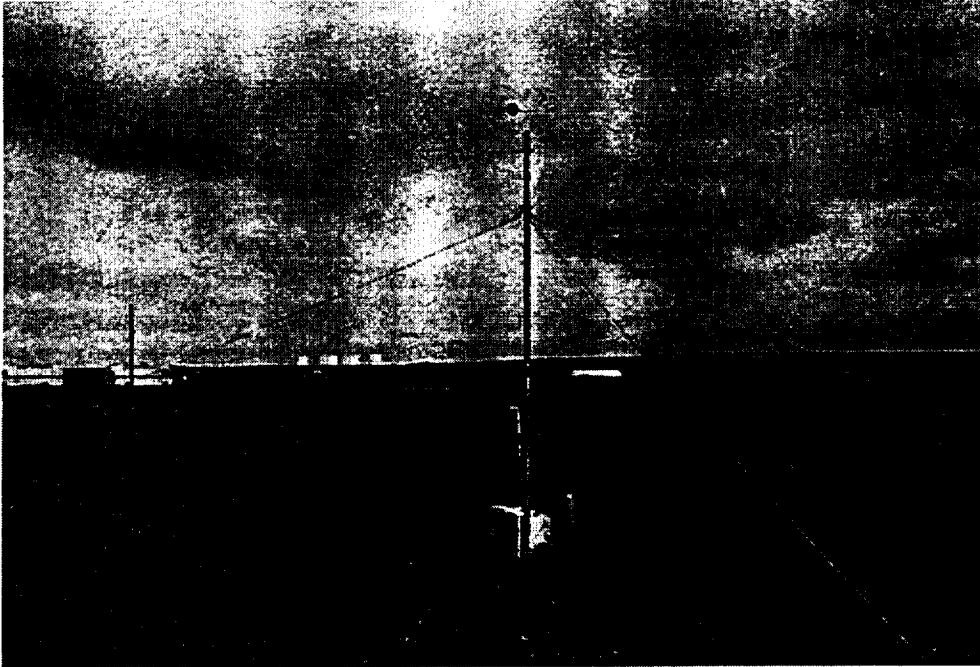
Figure 7. Microphone Tower for 4- and 12-foot Heights

Figure 8. Surface Microphone

All of the microphone positions and heights as well as the video camera and reference targets (discussed in Section 3.4) were surveyed. Geographical coordinates of key positions in the array were taken from U.S. Geographical Survey (USGS) maps, and confirmed by GPS averages over several days. Ground impedance was measured via an impedance tube.

Instrumentation at the end of the runway consisted of three microphones and a GPS-referenced IRIG-B time code recorded on a TEAC RD-145 multi-channel DAT recorder. Digitization rate for the DAT using four channels was 24,000 samples per second. Figure 9 shows the three microphones. The primary microphone was placed on a paving block on the ground. Unlike on-ground microphone positions in the main array, the objective was to obtain reference noise data; therefore, a ground board was appropriate. A second microphone was placed directly on the ground. A third microphone was placed on a four-foot high stand. The second and third microphones were deployed to obtain comparisons between these three microphone placements. In addition to the tape recordings, two digital integrating sound level meters were deployed. These were programmed in various modes, with their purpose being similar to that of the second and third tape-recorded microphones: comparisons between these instruments.

The location of the end of runway position was determined by long-term GPS averages.
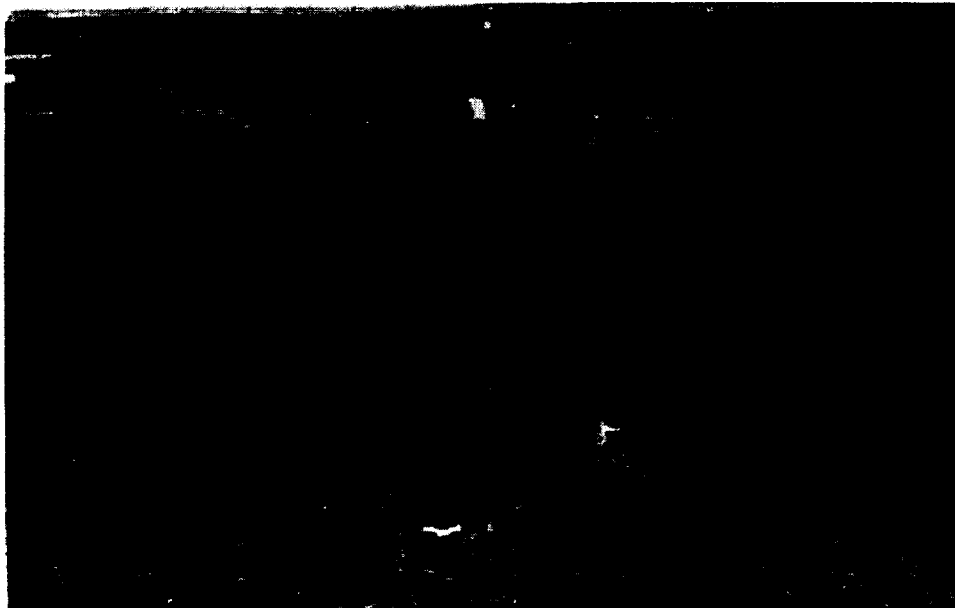
Figure 9. End-of-Runway Microphones

3.4 Aircraft Tracking

ARTS III radar data was obtained during this study. The flight plan portion of the ARTS data identified flights and their departure times, and the nominal aircraft type. The resolution of ARTS data was not adequate for analysis at the primary array, but was used at the less critical end of runway site.

A video camera was deployed at the position indicated in Figure 4. This was at a distance of 2725 feet from the runway centerline, and in line with the main microphone array. The camera was monochrome, with an 8.8 by 6.6 mm, 754 by 488 pixel CCD. Lens focal length was 8 mm, giving a nominal horizontal view angle of 58 degrees. Approximately 3000 feet of the runway was within the field of view. The camera was always leveled and pointed directly toward the runway, so that the CCD image plane was parallel to a vertical plane through the runway. Spatial resolution at the runway plane was about five feet.

The camera position was surveyed and marked, and always located at that position. Two targets were placed just below the south rim of the ravine, and their positions surveyed. These targets were used as references when analyzing video data, compensating for slight variations in camera aim and for jitter in digitization of video frames.

The video signal was recorded on a Hi 8 videocassette recorder. The time display from a GPS receiver was mixed into the video, and recorded together with the image. Figure 10 shows a typical video image, with the time code at the bottom and an aircraft taking off.

Figure 10. View of Site through Video Tracking Camera

3.5 Meteorological Data

Hourly surface weather data was obtained from DIA. This provided wind speed and direction, temperature, barometric pressure (as altimeter setting), dew point, precipitation and cloud cover and visibility. Upper-air atmospheric data was obtained from the twice-daily balloon launches at Denver Stapleton Airport. Because of the low altitudes involved, upper-air data was not used.

A 10-meter meteorological tower was deployed at the primary microphone site, recording wind speed at five heights, direction at three heights, and temperature at 10 heights. Figure 11 is a photograph of this tower. Data were recorded at two-second intervals.
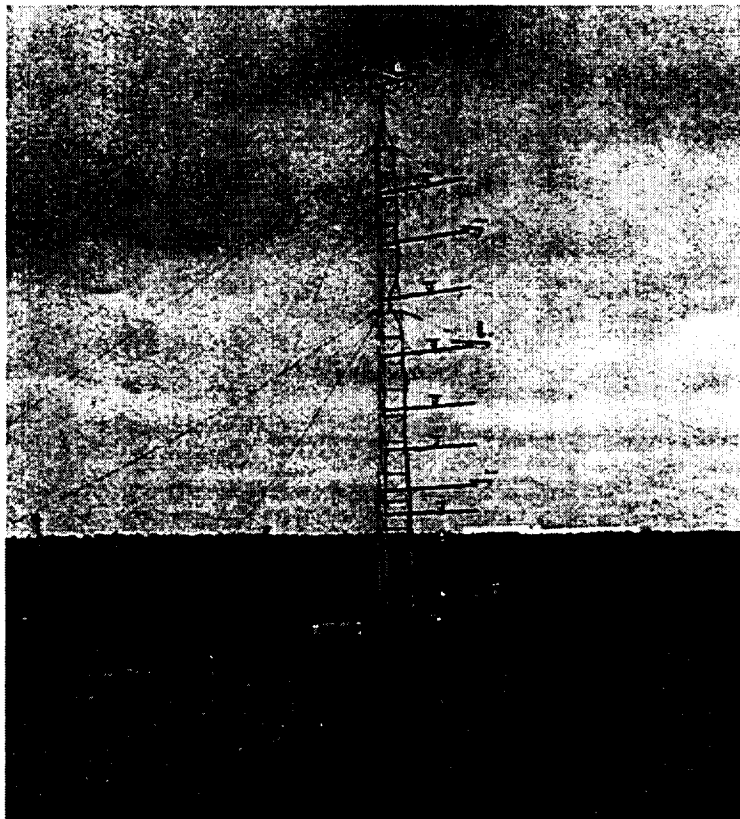
Figure 11. Meteorological Tower

3.6 Measurement Procedures

Measurements were made from 15 through 25 August 1997. Because of precipitation, no data was collected on 18, 23 and 24 August. Data collection was from 0800 to 1400 each day. That time period was selected to coincide with the busy morning period at the airport. During the six hours of collection each day, there were periods when aircraft would depart at intervals of one to two minutes, and periods when the runway was not active.

Calibration of all acoustical channels was conducted before and after each day's measurements. Test operations were controlled from the video camera position. Communication between the video position, the vans, and the end of runway position was by radio.

When an aircraft was observed turning onto the runway or beginning its takeoff roll, the test director would radio a "data on" command to the vans, and the recorders would be turned on. When the aircraft had passed and noise was low, a "data off" command was given. If aircraft were departing frequently, two or three departures might be recorded before ending the recording. A sequential run number, beginning with 101, was assigned to each recording. Runs up to number 800 were recorded. With multiple events, this corresponded to about 800 to 900 departures. An observer at the video position manually noted the time the aircraft passed the array and estimated its altitude. In the vans, the operators maintained manual logs of data start times, run numbers and gain settings, as a backup to the automatic recording of these parameters. Run numbers below 100 were used each day to identify pre- and post-test calibration records.

Radio communication with the end-of-runway position was intermittent. The recorder at this position was therefore operated independently. When the runway was active, the tape was allowed to run continuously. The TEAC places a sequential ID number (01 through 99) on the tape whenever a recording begins or whenever the "ID" front panel button is pressed. When the recorder was running continuously, the ID button was pressed each time an aircraft was observed to be rolling down the runway. This was generally 10 to 15 seconds before passing over the measurement position. ID numbers and overhead times were manually noted on a run log. Each event was thus assigned a run number that was different from the run numbers at the primary array. The time codes provided for absolute correlation of events.

4.0 Data Reduction and Processing

The objective was to analyze data for events with aircraft at various heights above the runway. Video tracking data was analyzed first, to determine which flights satisfied this need. Acoustic data was then analyzed for those flights.

4.1 Video Tracking Processing

Based on field notes of estimated aircraft height and review of the videotapes, 200 flights were selected for video analysis. These flights were selected primarily on the basis of obtaining a range of altitudes and also including a variety of aircraft. Because the primary array was at 6750 feet, rather than the design 8000 feet, aircraft were lower than had been desired. The 200 selections represented virtually all of the aircraft that were airborne, and some that were still on the ground as they passed the microphone position.

Each selected flight was played into a PC-based video capture card. Eight frames, at one-second intervals, were captured for each flight. Speeds were approximately 300 feet per second, so each of the eight frames contained the aircraft, with the aircraft just inside the picture at the first and last frame. The eight captured frames for each event were contained in a single multi-image TIFF file.

Each TIFF file was processed via specially written viewing software that allowed the user to mark two items on each frame:

- the aircraft position
- the two reference targets

Marking was done by positioning the mouse and clicking. Once a marker was in place, the program had the capability of "nudging" the marker one pixel at a time, using function and edit keys. With the five-foot video resolution noted earlier, and the one-pixel limit of the video analysis, aircraft position resolution was approximately 10 feet.

Figure 12 is a screen capture of this program. The target positions were marked with open circles, so that alignment with the reference targets could readily be observed. For each frame, the center of the aircraft was marked. Figure 12 shows one frame after the

aircraft position had been marked in all eight frames. All eight of the position markers (open circles) are shown. The targets and registration markers (white circles) are seen near the left and right edges. Other lines on the figure (dashed line above the aircraft; solid line and filled circle off the frame to the left) are track calculations based on the ARTS radar data. Because the first radar point occurred very often when the aircraft was well past the primary microphone position, tracking from those data usually required extrapolation. The result was accuracy poorer than ARTS radar's basic resolution of 1/8 nautical mile horizontally and 100 feet vertically. Times from the radar data were generally within one to two seconds of times from the time code generator.

After all eight frames were digitized for an event, the analysis program computed the time the aircraft passed the microphone array, its altitude, and its climb angle. This was written to a small file, one file per event.
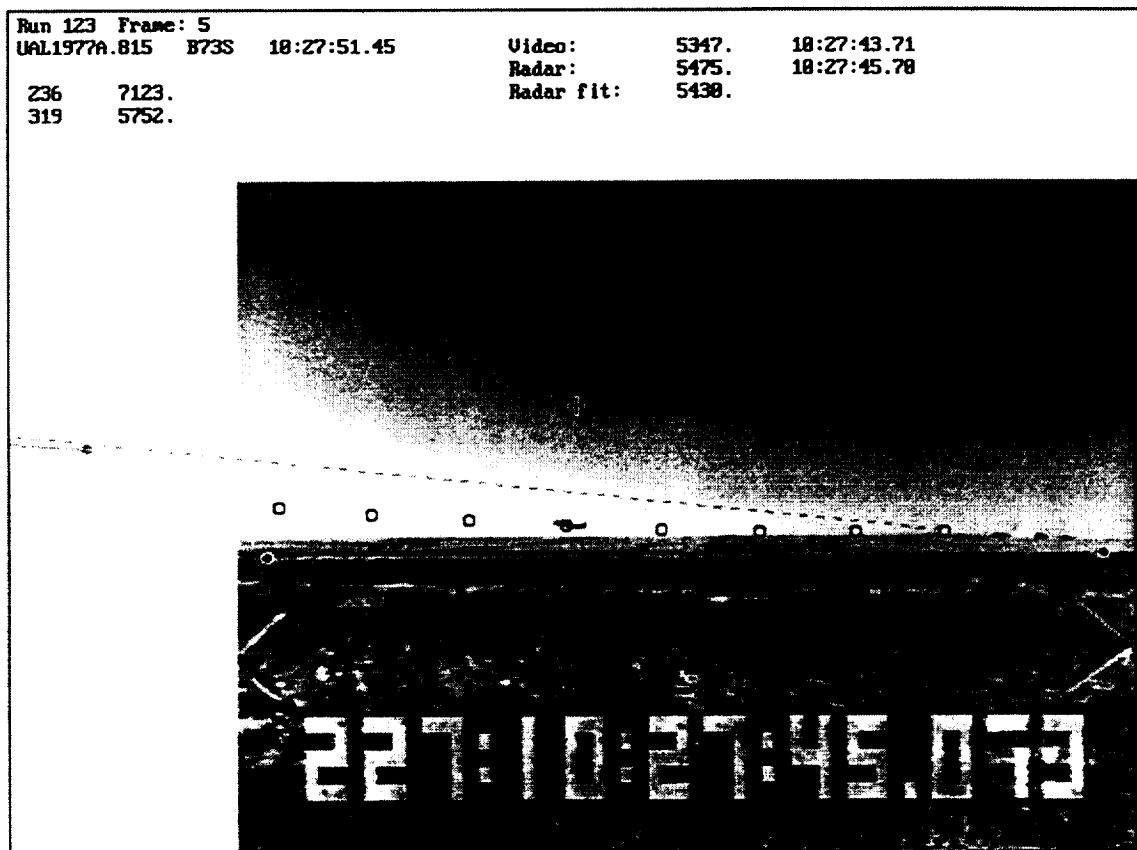
Figure 12. Example Analysis of Video Tracking Data

4.2 Primary Array Acoustic Data

After each day's data collection, noise data were processed into one-third octave band spectra at one-quarter second intervals. Processing was performed on a PC equipped with an 8-mm tape drive. An automated software system was set up which would transfer each run to the PC and perform the processing. The procedure for obtaining the spectra was:

1. Run number, gain settings and times were read from the beginning of each run.

2. File record numbers corresponding to even one-quarter-second times were computed.

3. For each one-quarter-second period, 5120 samples of each channel were taken from the file. These 5120 samples were divided into five 1024-sample blocks. An FFT was taken of each block, then processed into a 400-line power spectrum. A Hanning window was applied to each FFT block.

4. The five power spectra were summed. The summed spectrum was then processed into a one-third-octave spectrum. The one-third-octave spectral bands had "wall" (vertical slope) skirts. Lines adjacent to the band edges were apportioned between the bands.

A-weighted and overall sound pressure levels were computed for each one-quarter-second interval. These levels and the one-third-octave spectra were written to a file in ASCII format. A small header at the top of each file contained time and other reference information. Each file contained all six channels from one van, so there were two files per run. File names included the run number and identification of the van.

This processing took place for all runs, on a daily basis during the measurements.

After video processing identified which events were to be analyzed, the one-third-octave spectrum files for those events were divided and/or rewritten into smaller files, one for each takeoff to be analyzed, containing noise data associated with a single event. The time span to be included for each event was determined by displaying the time history of the A-weighted level, overall level, and spectra via a specially written interactive program, and adjusting cursors to delimit the event period. All 12 channels from each run were merged into a single file, retaining data only within the user-selected limits. Each file was

named according to the number of the run as assigned during measurements. Events that were part of multi-takeoff recordings had a sequential letter appended to the run number. This final set of files – one file per event, all microphone channels, extraneous data before and after the aircraft noise event deleted – are referred to as "event files", and were also given type extension "EVT".

After EVT files were prepared for the 200 flights, the data was qualified. The objective was to include only data with signal (maximum level and SEL)-to-noise (ambient) ratio of at least 10 dB. Events, which did not satisfy this criterion (other than perhaps a few one-third-octave bands), were excluded. After this review, 162 events remained.

Table 1 lists the 162 events. The table includes pertinent information about each flight, plus surface meteorological data. The meteorological data is that recorded at the beginning of the hour containing the event.

Table 4-1. Summary of Flights Analyzed

Run	Flight	Date (mdd)	Time[1] (local)	ACType	Zmsl[2] feet	Zagl[3] feet	Climb[4] deg	Temp deg F	RH %	Wind Kt	Wdir deg
123	ual1977	815	10:27:43.7	B73S	5347	30	1.601	75	30	9	200
125	ual1078	815	10:31:24.6	B757	5356	39	1.652	75	30	9	200
162	dal432	816	8:01:33.6	B757	5363	46	0.945	59	88	8	030
163	kmr188	816	8:13:26.7	B73S	5362	45	1.658	59	88	6	010
165A	aal834	816	8:18:50.8	MD80	5342	25	0.742	59	88	6	010
167B	ual1598	816	8:27:02.6	B737	5338	21	0.000	57	87	7	360
168	ual1145	816	8:30:01.0	B73J	5514	197	7.397	57	87	7	360
170	ual1491	816	8:33:42.0	B73J	5385	68	3.377	57	87	7	360
172	ual484	816	8:41:01.5	B73J	5383	66	4.384	57	87	7	360
175	ual1660	816	8:53:46.5	B73J	5351	34	1.696	57	94	5	VRB
178A	kmr19	816	9:09:57.9	B73S	5536	219	10.146	57	94	5	VRB
180	kmr273	816	9:17:12.5	B73S	5388	71	2.498	57	94	5	VRB
185	dal334	816	9:41:08.3	B757	5367	50	2.553	57	94	5	VRB
186	ual222	816	9:53:40.9	B757	5343	26	0.000	63	77	3	VRB
195B	ual1274	816	10:47:45.7	B73J	5380	63	3.400	63	77	3	VRB
215A	UAL1043	816	12:33:17.2	B73J	5510	193	7.326	70	62	4	VRB
217	UAL1430	816	12:37:02.2	EA32	5350	33	1.701	70	62	4	VRB
218A	UAL1124	816	12:38:27.0	B73S	5385	68	3.356	70	62	4	VRB
218B	UAL796	816	12:39:40.2	B737	5340	23	1.005	70	62	4	VRB
231	UAL8154	816	13:12:00.5	B777	5372	55	2.603	70	62	6	360
232	DAL244	816	13:13:52.4	B757	5372	55	3.400	70	62	6	360
235	UAL1580	816	13:18:52.3	B757	5354	37	0.737	70	62	6	360
236	DAL2120	816	13:24:43.8	B727	5340	23	0.000	70	62	6	360
238	FFT776	816	13:40:48.7	B737	5340	23	0.000	70	62	6	360
241	UAL1606	816	13:50:34.3	B73J	5359	42	1.730	70	62	6	360
243	DAL432	817	7:55:08.3	B757	5452	135	4.946	57	94	10	100
244	USA120	817	7:58:08.3	B73F	5334	17	0.000	57	94	10	100
245	AAL858	817	8:04:06.0	B757	5399	82	4.473	57	94	10	100
247	COA334	817	8:34:21.9	MD80	5341	24	0.991	57	94	10	100
253	UAL1762	817	9:05:12.8	B727	5338	21	0.000	63	77	14	140
255	DAL1227	817	9:10:03.3	B727	5339	22	0.865	63	77	14	140
260	UAL1474	817	9:22:23.2	B757	5343	26	0.945	63	77	12	130
261	NWA566	817	9:26:39.2	B757	5517	200	7.224	63	77	12	130
263	NWA1224	817	9:31:49.5	B727	5336	19	0.000	63	77	12	130
272	UAL1184	817	10:24:52.9	B73J	5519	202	10.359	64	72	17	140
276	UAL8187	817	10:37:15.0	B757	5373	56	3.457	64	72	17	140
277B	UAL1576	817	10:40:50.5	EA32	5356	39	2.654	64	72	17	140
281A	UAL336	817	10:51:22.9	B727	5336	19	0.000	64	72	17	140
282	UAL766	817	10:54:37.8	B757	5365	48	2.654	70	62	15	150
285A	AWI570	817	11:07:34.2	BA46	5455	138	5.614	70	62	15	150
286	DAL1716	817	11:11:02.8	B757	5454	137	6.798	70	62	15	150
294	NWA564	817	11:57:58.2	B757	5455	138	7.005	73	52	13	180
302	UAL1200	817	12:50:27.6	B757	5342	25	0.000	73	52	13	180
303	UAL724	817	12:52:00.6	B757	5379	62	2.736	73	52	13	180
304	UAL8135	817	12:54:09.6	B777	5367	50	0.746	75	45	11	160
305	DAL244	817	12:59:26.1	B757	5442	125	7.197	75	45	11	160
308	UAL8154	817	13:25:22.5	B777	5366	49	2.654	75	45	11	160
322	NWA566	819	9:12:59.6	B757	5450	133	8.130	63	58	12	220
328	NWA802	819	9:37:55.8	EA32	5380	63	4.355	63	58	12	220
334	AWI588	819	10:22:55.8	BA46	5375	58	2.907	73	39	3	250
335C	UAL1977	819	10:28:39.4	B73S	5362	45	1.631	73	39	3	250
337	UAL766	819	10:31:30.8	B757	5353	36	1.658	73	39	3	250
339	UAL1184	819	10:34:09.5	B73J	5375	58	2.736	73	39	3	250
347A	KMR118	819	10:52:34.9	B73S	5551	234	8.412	73	39	3	250
347B	KMR340	819	10:53:34.5	B73S	5385	68	4.355	73	42	6	030
349	AAL1080	819	11:01:01.7	B757	5397	80	5.477	73	42	6	030
350	KMR440	819	11:02:32.8	B73S	5448	131	6.233	73	42	6	030
353	AWI610	819	11:07:25.3	BA46	5367	50	3.082	73	42	6	030
357	DAL1716	819	11:25:58.7	B757	5459	142	8.612	73	42	6	030
361B	KMR465	819	11:50:07.8	B73S	5631	314	9.605	73	42	6	030

Table 4-1. Summary of Flights Analyzed (Continued - 2 of 3)

Run	Flight	Date (mdd)	Time (local)	ACType	Zmsl feet	Zagl feet	Climb deg	Temp deg F	RH %	Wind Kt	Wdir deg
367	UAL8877	819	12:11:08.1	B73S	5416	99	5.881	72	49	15	040
369	UAL1124	819	12:28:00.5	B73S	5380	63	2.620	72	49	15	040
370	UAL2761	819	12:29:18.3	B73S	5442	125	5.611	72	49	15	040
371	UAL1043	819	12:30:47.0	B73J	5488	171	8.186	72	49	15	040
379	UAL1296	819	12:47:22.1	B757	5449	132	7.005	72	49	15	040
381	UAL1200	819	12:50:19.0	B757	5349	32	0.945	72	49	15	040
383	UAL1622	819	12:54:15.8	B73S	5359	42	1.707	72	49	15	040
383B	UAL724	819	12:55:06.8	B757	5356	39	1.759	72	49	15	040
384	UAL1688	819	12:56:46.8	B73S	5346	29	0.868	72	49	15	040
385	UAL8135	819	12:58:29.7	B777	5370	53	3.515	72	49	15	040
395	UAL1168	819	13:46:36.6	B73J	5390	73	3.541	72	49	15	040
396	DAL244	819	13:52:49.1	B757	5401	84	4.163	72	49	15	040
402A	ual1491	820	8:47:56.3	B73J	5415	98	5.386	61	77	7	260
403	aal1664	820	9:03:43.7	MD80	5350	33	0.000	63	77	7	270
406B	kmr19	820	9:12:43.2	B73S	5537	220	9.652	63	77	7	270
411	DAL334	820	9:34:08.4	B757	5367	50	4.176	63	77	7	270
413	nwa802	820	9:44:09.0	EA32	5395	78	5.194	63	77	7	270
414	ual2755	820	9:57:46.7	B73J	5372	55	2.726	66	63	7	300
416	ual1977	820	10:18:58.7	B73S	5419	102	5.064	66	63	7	300
418	ual1500	820	10:22:01.6	B73J	5404	87	6.175	66	63	7	300
420B	ual1078	820	10:29:26.1	B757	5355	38	1.626	66	63	7	300
421	ual2757	820	10:30:56.5	B73S	5415	98	4.271	66	63	7	300
423	aal1080	820	10:33:40.6	B757	5465	148	9.168	66	63	7	300
426B	ual1184	820	10:42:54.2	B73J	5365	48	2.645	66	63	7	300
426C	kmr170	820	10:43:46.0	B73S	5358	41	2.537	66	63	7	300
429A	kmr440	820	10:48:07.0	B73S	5379	62	3.302	66	63	7	300
429B	kmr494	820	10:48:58.9	B73S	5368	51	4.271	66	63	7	300
431	n142b	820	10:53:56.3	CL61	5625	308	7.528	70	54	3	340
433A	kmr340	820	10:57:08.7	B73S	5382	65	5.228	70	54	3	340
433B	kmr118	820	10:57:55.6	B73S	5445	128	6.150	70	54	3	340
435	ual200	820	11:05:50.7	EA32	5347	30	0.759	70	54	3	340
436	ual8101	820	11:14:31.9	B777	5349	32	0.000	70	54	3	340
437	ual1102	820	11:16:19.5	B757	5343	26	0.000	70	54	3	340
439	ual1728	820	11:21:44.2	B73S	5350	33	2.039	70	54	3	340
441B	ual2759	820	11:38:45.2	B73J	5355	38	2.611	70	54	3	340
444	dal1716	820	11:44:19.7	B757	5349	32	1.631	70	54	3	340
448	aal1008	820	11:57:39.8	MD80	5346	29	0.769	73	45	0	000
458	ual1124	820	12:39:25.6	B73S	5436	119	6.71	73	45	0	000
460	ual1146	820	12:42:52.0	B73J	5343	26	0.907	73	45	0	000
461	ual586	820	12:44:51.3	B73J	5363	46	3.600	73	45	0	000
462	ual8154	820	12:45:58.0	B777	5349	32	0.000	73	45	0	000
465	ual1296	820	12:51:12.2	B757	5385	68	4.488	73	45	0	000
466	ual1430	820	12:52:44.8	EA32	5348	31	1.631	73	45	0	000
467B	ual1043	820	12:54:41.6	B73J	5396	79	4.355	75	42	5	060
469	ual1580	820	12:57:25.0	B757	5405	88	4.630	75	42	5	060
470	ual724	820	12:58:48.3	B757	5364	47	2.645	75	42	5	060
472	ual1802	820	13:04:01.9	B73J	5352	35	0.744	75	42	5	060
476	ABX2377	821	9:00:10.3	DC8	5345	28	0.807	66	63	8	280
477	KMR19	821	9:18:52.1	B73S	5628	311	9.849	66	63	8	280
478	AAL834	821	9:19:56.6	MD80	5513	196	7.125	66	63	8	280
479	DAL1066	821	9:21:24.5	B767	5380	63	4.428	66	63	8	280
505	UAL8154	821	12:42:46.7	B777	5370	53	2.690	82	30	7	270
506	UAL586	821	12:45:08.5	B73J	5371	54	2.498	82	30	7	270
512	UAL1580	821	13:02:33.4	B757	5413	96	5.714	86	22	3	270
515	DAL244	821	13:07:42.1	B757	5385	68	3.250	86	22	3	270
524A	UAL1606	821	13:39:53.9	B73J	5350	33	1.660	86	22	3	270
526	KMR266	821	13:44:52.4	B73S	5483	166	5.247	86	22	3	270
528	USA120	822	7:55:12.7	B73S	5345	28	0.000	63	66	3	140
530	ABX2377	822	8:11:41.5	DC8	5360	43	1.809	63	66	3	140

Table 4-1. Summary of Flights Analyzed (Concluded - 3 of 3)

Run	Flight	Date (mdd)	Time (local)	ACType	Zmsl feet	Zagl feet	Climb deg	Temp deg F	RH %	Wind Kt	Wdir deg
533	FDX3209	822	8:23:51.7	EA30	5418	101	5.177	63	66	3	140
534A	UAL484	822	8:25:50.4	B73S	5377	60	2.425	63	66	3	140
535	UAL1726	822	8:27:33.6	B73J	5388	71	4.327	63	66	3	140
536	KMR188	822	8:30:06.3	B73S	5360	43	0.735	63	66	3	140
538	UAL180	822	8:35:32.9	B757	5368	51	1.581	63	66	3	140
543	DAL432	822	8:43:17.3	B757	5377	60	3.474	63	66	3	140
544	FFT902	822	8:58:58.4	B737	5348	31	0.958	70	50	7	250
547B	NWA566	822	9:14:22.7	B757	5548	231	8.448	70	50	7	250
548	UAL240	822	9:15:51.7	B777	5379	62	3.698	70	50	7	250
551B	DAL334	822	9:33:21.3	B757	5427	110	5.837	70	50	7	250
558	UAL1078	822	10:22:58.6	B757	5391	74	3.445	75	36	3	VRB
561	UAL1184	822	10:28:51.2	B73J	5534	217	7.775	75	36	3	VRB
562	UAL548	822	10:30:33.2	B757	5366	49	0.942	75	36	3	VRB
564A	UAL396	822	10:34:41.2	B73S	5372	55	2.681	75	36	3	VRB
566	AWI580	822	10:42:12.0	BA46	5350	33	0.000	75	36	3	VRB
567C	KMR440	822	10:48:04.2	B73S	5368	51	3.485	75	36	3	VRB
570A	FFT540	822	10:53:29.1	B73S	5408	91	5.856	79	29	7	070
570B	KMR48	822	10:54:25.5	B73S	5429	112	6.212	79	29	7	070
573	FFT660	822	10:58:58.4	B737	5378	61	3.588	79	29	7	070
576	DAL1716	822	11:12:19.4	B757	5421	104	6.058	79	29	7	070
586A	KMR465	822	11:47:49.7	B73S	5539	222	10.596	79	29	7	070
601A	UAL1610	822	12:50:49.8	B73J	5415	98	5.440	81	28	6	050
611	DAL244	822	13:35:03.0	B757	5413	96	6.582	82	26	4	VRB
612B	UAL1606	822	13:38:37.9	B73J	5393	76	6.037	82	26	4	VRB
613A	UAL1168	822	13:39:47.5	B73J	5419	102	3.900	82	26	4	VRB
615	KMR266	822	13:47:11.4	B73S	5520	203	7.871	82	26	4	VRB
714	FFT902	825	9:03:26.2	B737	5376	59	2.529	73	48	6	240
719	FFT643	825	9:13:49.9	B73S	5353	36	0.692	73	48	6	240
725	DAL334	825	9:40:04.1	B757	5404	87	5.112	73	48	6	240
736	AAL1080	825	10:32:24.8	B757	5354	37	0.000	79	36	6	010
739A	FFT660	825	10:37:10.5	B737	5370	53	2.812	79	36	6	010
740A	KMR494	825	10:40:56.2	B73S	5390	73	5.026	79	36	6	010
740B	KMR48	825	10:41:41.6	B73S	5367	50	2.519	79	36	6	010
743B	KMR170	825	10:46:09.7	B73S	5451	134	5.350	79	36	6	010
748B	KMR118	825	10:55:31.6	B73S	5508	191	7.125	82	32	7	020
750	KMR340	825	11:02:21.9	B73S	5457	140	7.054	82	32	7	020
752	DAL1716	825	11:06:17.1	B757	5385	68	4.150	82	32	7	020
761	KMR161	825	11:36:14.5	B73S	5391	74	2.731	82	32	7	020
765B	KMR465	825	11:45:15.1	B73S	5520	203	10.388	82	32	7	020
789	DAL244	825	13:06:32.5	B757	5395	78	4.285	86	25	5	VRB
796A	AAL1438	825	13:37:22.9	MD80	5356	39	1.701	86	25	5	VRB
797	FFT542	825	13:39:28.3	B73S	5365	48	2.490	86	25	5	VRB
800	KMR262	825	13:44:50.5	B73S	5348	31	0.945	86	25	5	VRB

Notes:

[1]Time = time aircraft passed primary microphone array

[2]Zmsl = altitude, feet MSL, as aircraft passed primary array

[3]Zagl = altitude, feet AGL, as aircraft passed primary array

[4]Climb = climb angle

4.3 End-of-Runway Acoustic Data

After completion of the tests, acoustic data were transferred from DAT to a PC via an interface special to the TEAC RD-145. Each record was placed in its own file. The transferred data, in a TEAC proprietary multi-channel format, were then processed into single-channel WAV files. The WAV file containing IRIG-B time code was processed to establish the time as a function of position within each file. WAV files were then processed into one-third-octave spectra at one-quarter-second intervals, by the same procedure as described in Section 4.1. Because of the different sampling rate (24000/second versus 20000/second), each interval was constructed from three 2048 point FFTs.

Using the time to correlate events, the spectral file for each ID event (these were strictly one flyover per file) was renamed to include the event number used at the primary microphone array. These files (with extraneous before and after data trimmed off) represented event files at the end-of-runway position. This processing was done for the 162 events listed in Table 1.

5.0 Analysis

5.1 Spectral Analysis of Selected Events

A major hypothesis of the current study is that the theories of References 6 and 14 through 17 correctly describe the effect of the ground on aircraft noise propagation. Ultimately, simple relations like those of References 3, 4 and 5 have great practical benefits, but the hypothesis must be tested against full spectral results.

The initial phase of analysis was therefore to compare measured spectra with predictions from the full EGA theory. During this phase, it was very desirable to avoid as many uncertain details as possible. Analysis was therefore performed via differences between microphones, so that it would not be necessary to predict the source noise spectrum of each aircraft. Analysis was also performed for noise corresponding to propagation along the microphone array. This ensured that propagation would always involve sound radiated at a direction 90 degrees to the aircraft's axis, avoiding complications of directivity relative to the flight path. Source directivity about the roll axis (shielding of Reference 3) could still be an issue, but for a given aircraft elevation the difference in roll-axis direction to all microphones in the array would be less than 25 degrees; half that if comparisons were limited to adjacent pairs of microphone distances. Comparisons between the three microphones at a given distance involved roll-axis differences of less than two degrees.

This analysis was performed for selected flights. For each case, losses due to spherical spreading, air absorption and ground effect were computed, and added to the measured third octave spectra. If all effects were perfectly modeled, then the adjusted data would collapse to a single spectrum. To assess ground effect theory, adjustments were performed in two stages. First, inverse spreading and air absorption were applied, and differences between spectra noted. Second, ground effect was applied, and improvement to the collapse was noted.

When spectra were compared for the three heights at a single distance, it was not necessary to adjust for air absorption and spherical spreading. Detailed comparisons were also made for calm conditions, so that refraction effects were not expected to be a major factor.

The comparisons presented in this section are for one-quarter-second average one-third-octave-band spectra. They correspond to propagation of sound generated as the aircraft pass the microphone array. Timing of the measured noise allows for the source location being somewhat to the rear of the aircraft, and for the propagation time from the aircraft to the receiver. EGA calculations used a flow resistivity of 200 rayls.

Figure 13 shows measured spectra at three microphones at 666 feet for one flight, with an aircraft 30 feet above the ground. This spectrum is for a one-quarter-second period, and the source is in line with the microphone. The elevation angle from the aircraft to the ground at the microphones is 2.6 degrees. Differences between the three microphone heights are at higher frequencies, 400 Hz and above. Note that, for the 12-foot microphone, there is a minimum at around 250 Hz and a maximum at around 500 Hz. These features correspond to the full argument of the cosine term of Equations (10) and (11), not just Δr.
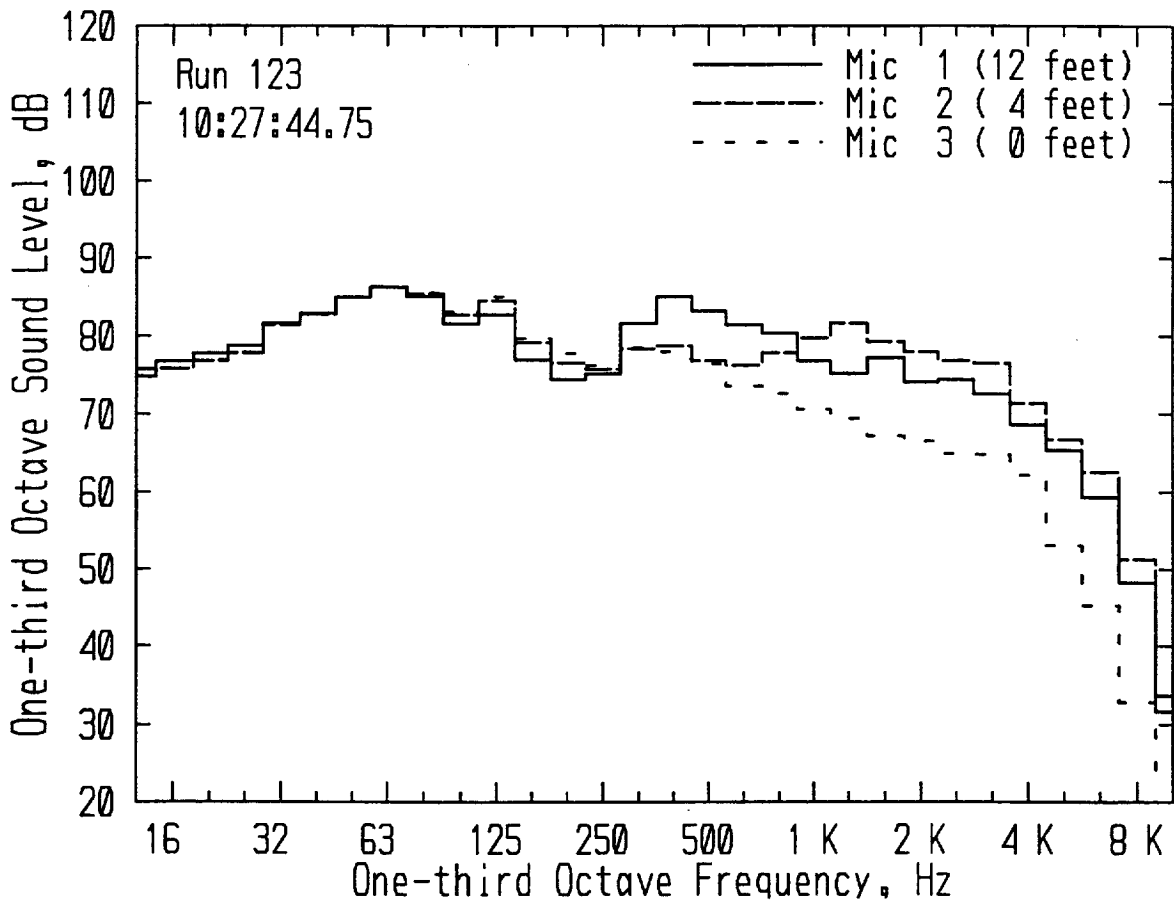
Figure 13. Measured Spectra, Aircraft Height 30 Feet, Distance 666 Feet

Figure 14 shows the same data, but with propagation effects (EGA theory) adjusted. The three spectra are now in good agreement at most frequencies, although there are some mismatches, such as the spike in the 4-foot microphone at 3150 Hz. The spectra also no longer show the interference pattern seen in Figure 13.
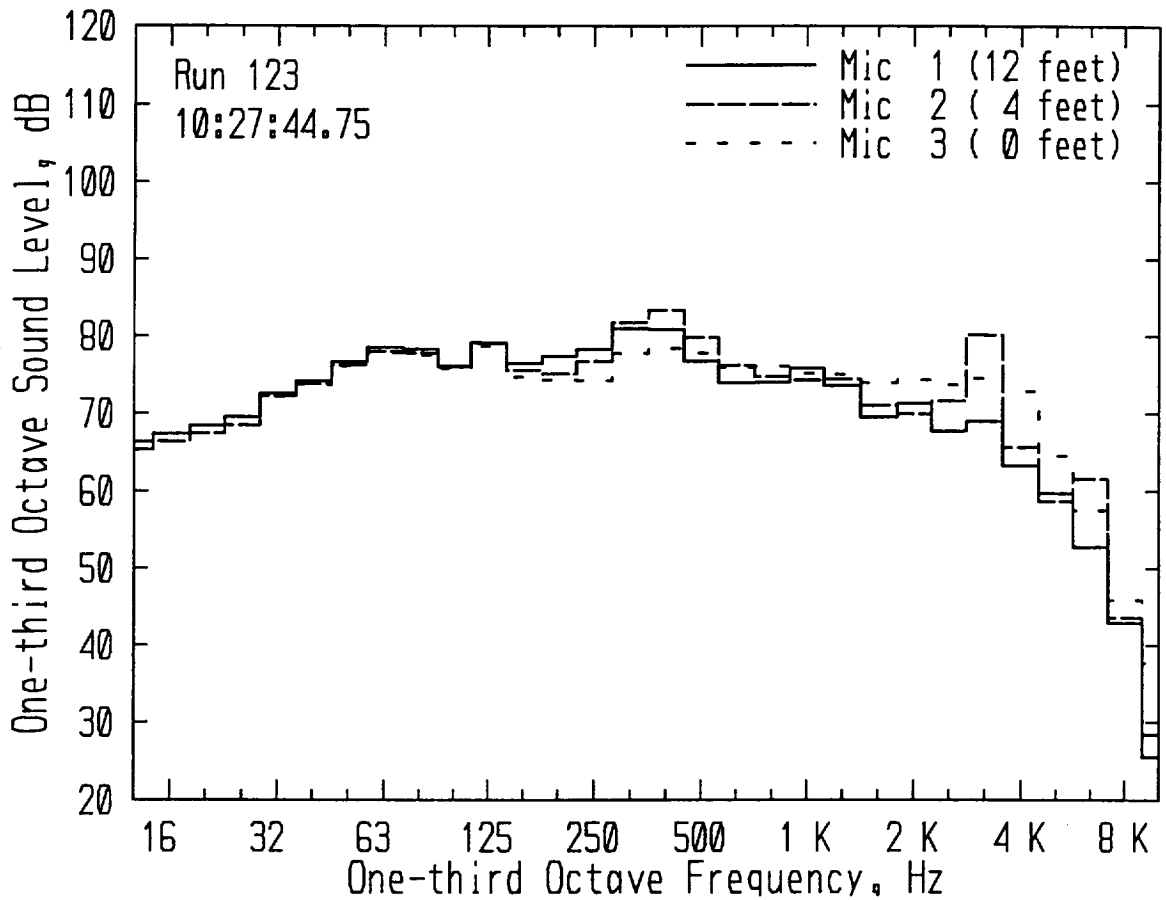
Figure 14. Propagation-adjusted Spectra, Aircraft Height 30 Feet, Distance 666 Feet

Figure 15 shows measured spectra from the same flight (altitude 30 feet) as measured at the three 1000 foot microphones with elevation angle of 1.7 degrees. Spectra at the three heights coincide up to through the 315 Hz band, then differ substantially at higher frequencies. An interference dip is seen around 200 Hz.
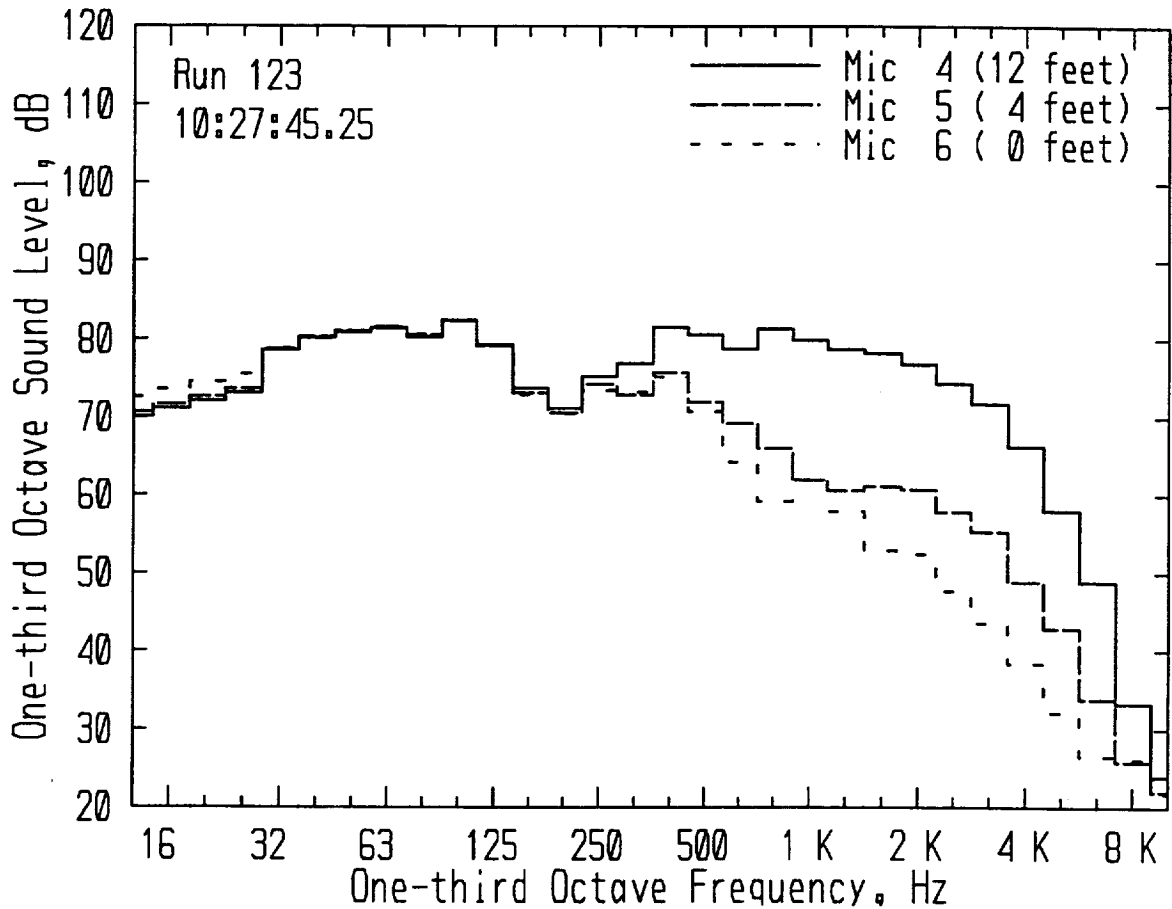
Figure 15. Measured Spectra, Aircraft Height 30 Feet, Distance 1000 Feet

Figure 16 shows the 1000-foot spectra adjusted for ground effect (EGA theory). The spectra are in reasonable agreement through the 800 Hz band, and the interference minimum at 200 Hz is no longer prominent. Spectra still disagree above 1000 Hz, but differences are somewhat less.
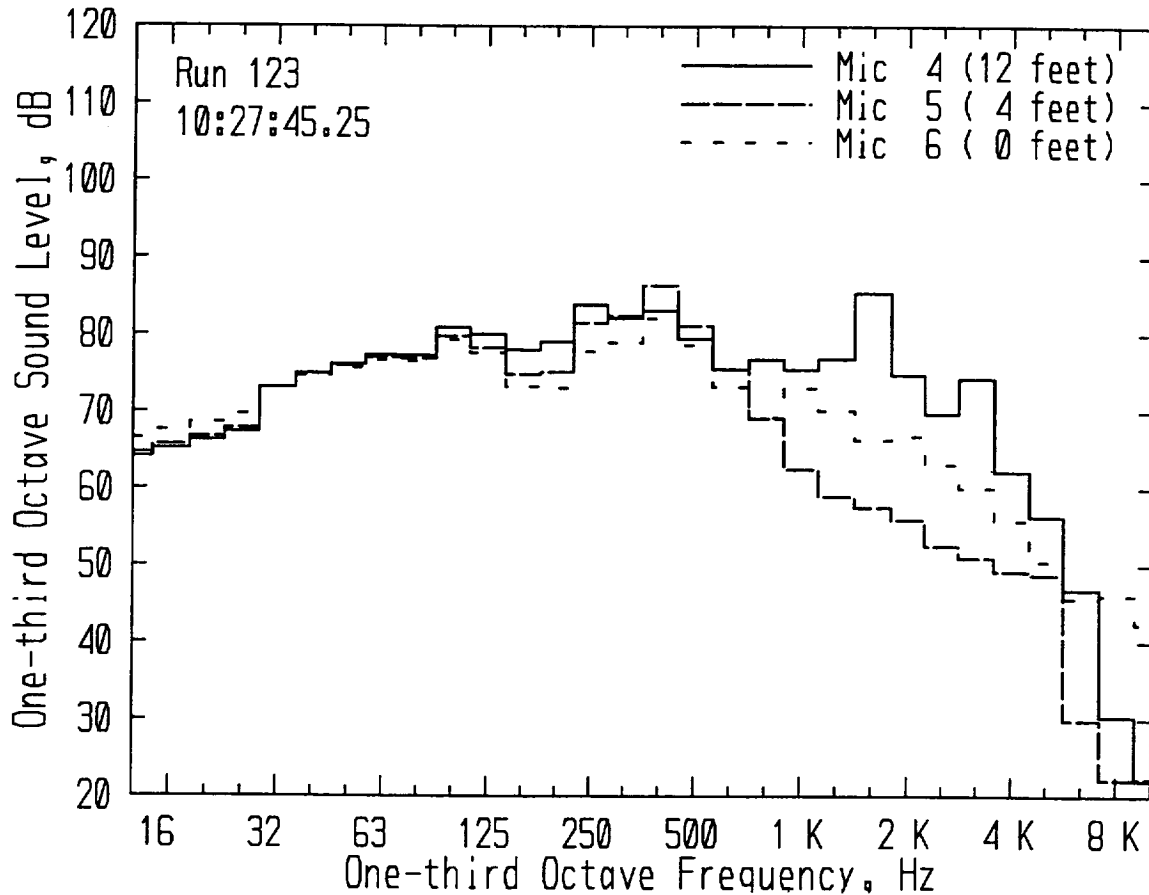
Figure 16. Propagation-adjusted Spectra, Aircraft Height 30 Feet, Distance 1000 Feet

Figures 17 and 18 show a similar comparison for an aircraft 140 feet above the ground, and receiver distance of 1500 feet, with elevation angle of 5.3 degrees. As with the 666- and 1000 foot examples, differences are primarily at higher frequencies. Note that adjustment for ground effect brings the spectra into closer agreement than was seen at the 1000-foot position.

Figures 19 and 20 show the 140-foot flyover at a distance of 2000 feet. Features are similar to those seen at the other three distances.
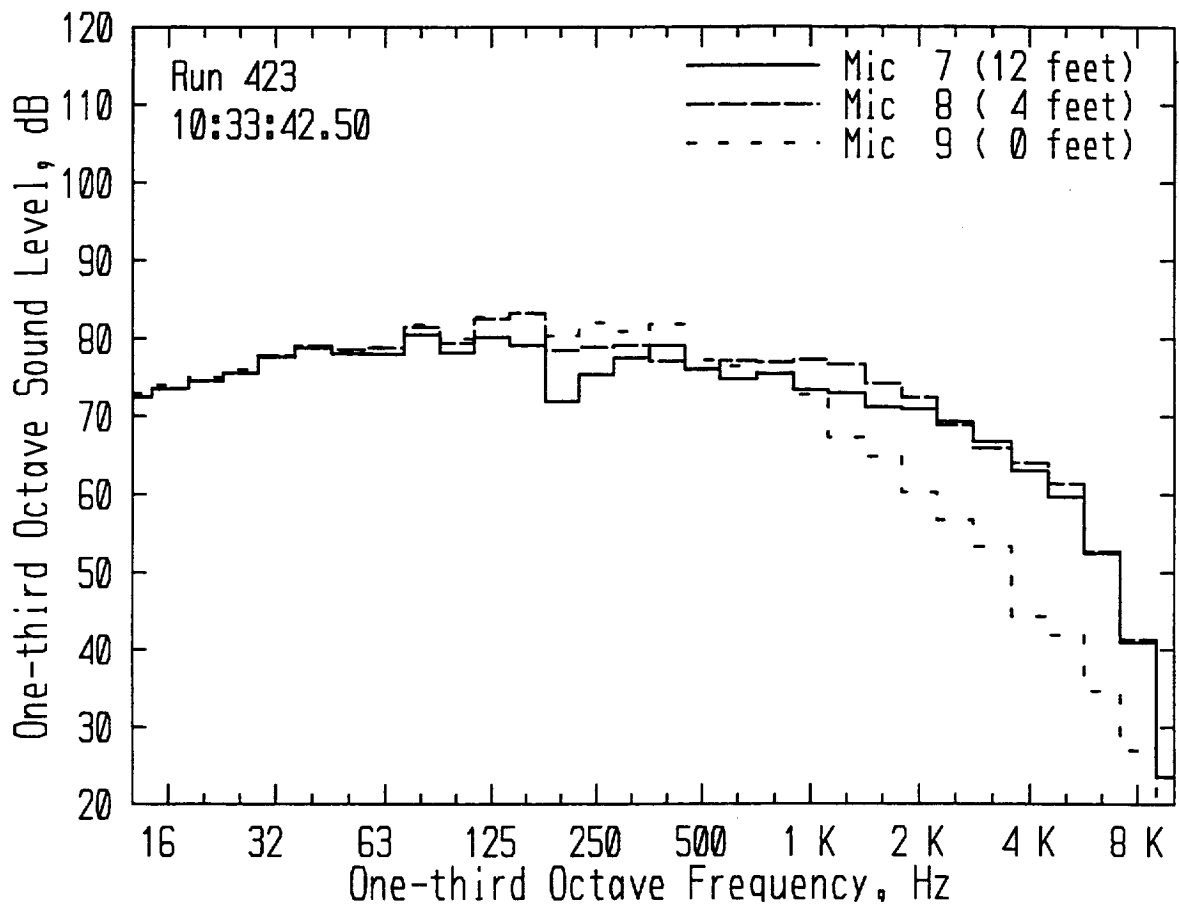
Figure 17. Measured Spectra, Aircraft Height 140 Feet, Distance 1500 Feet
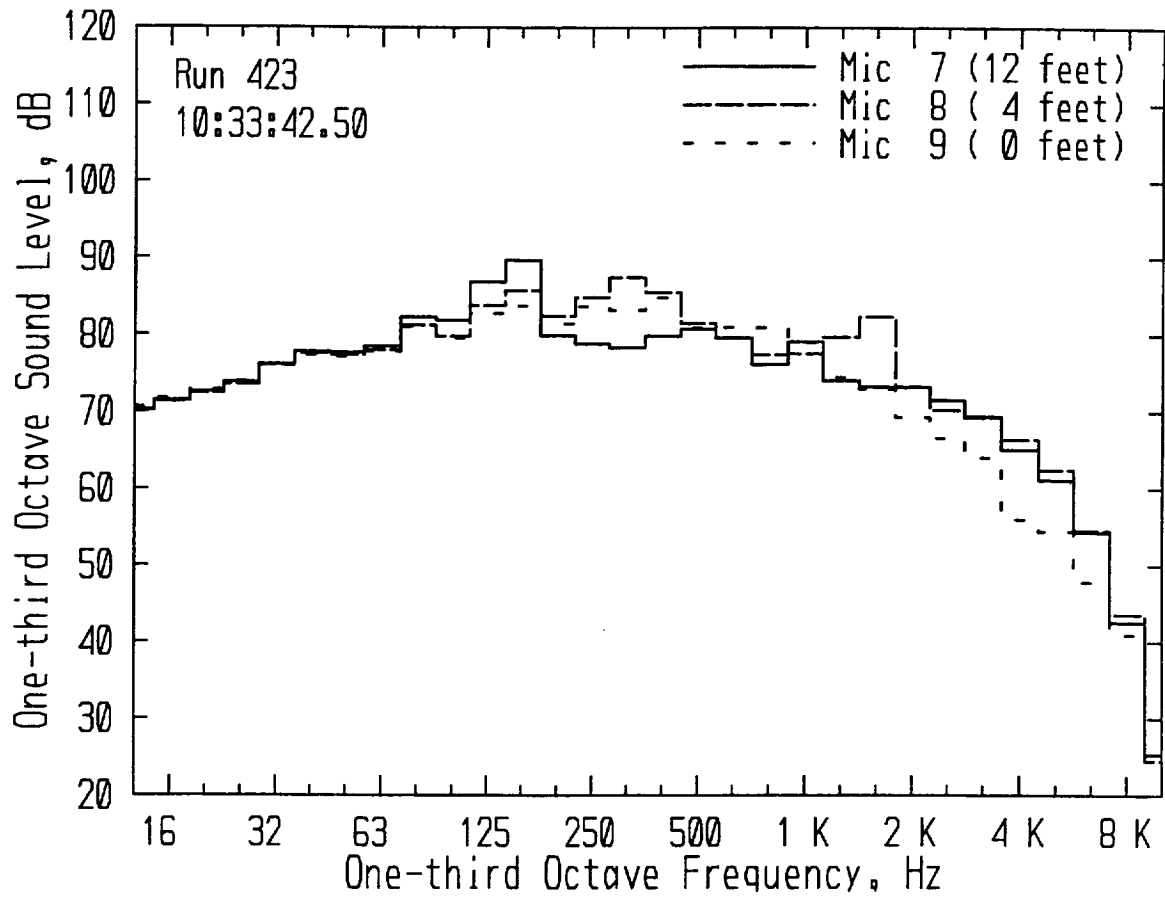
Figure 18. Propagation-adjusted Spectra, Aircraft Height 140 Feet, Distance 1500 Feet
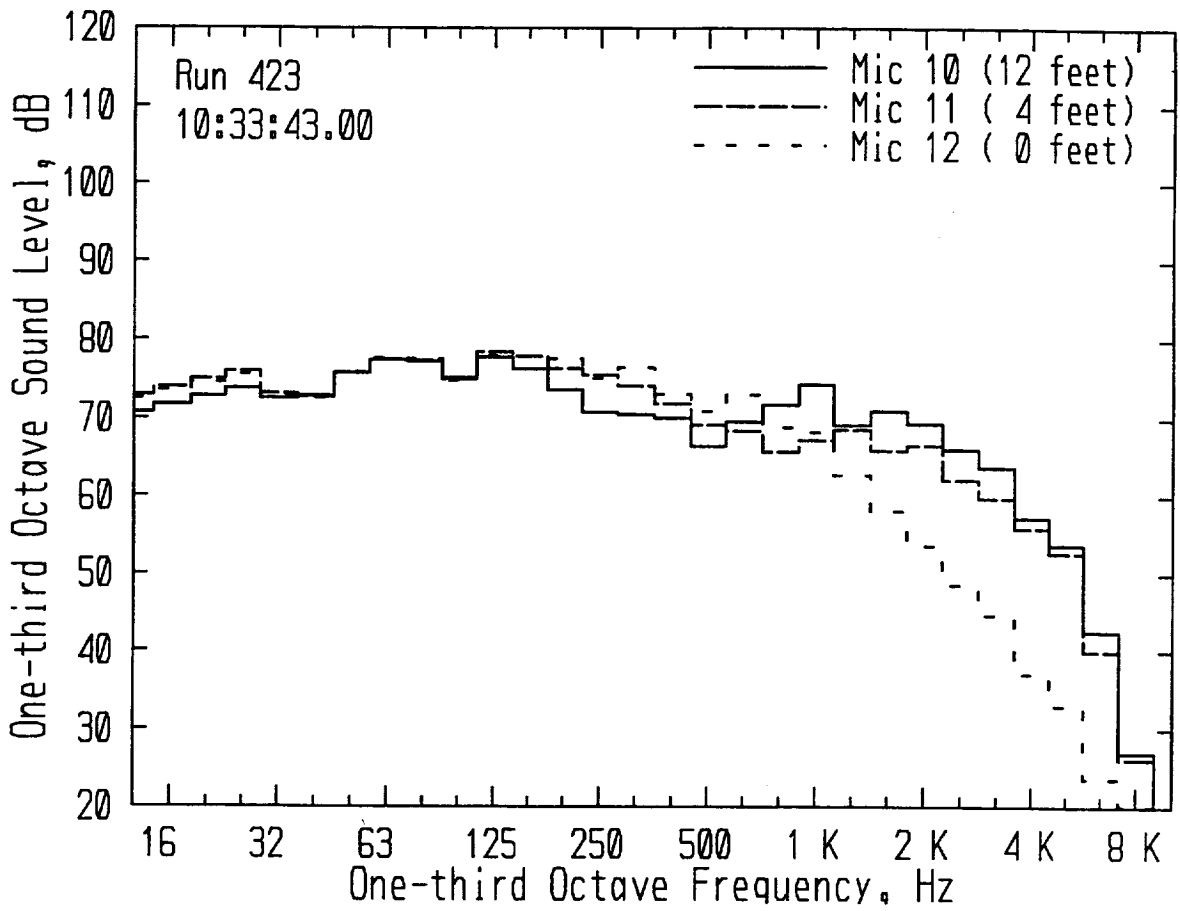
Figure 19. Measured Spectra, Aircraft Height 140 Feet, Distance 2000 Feet
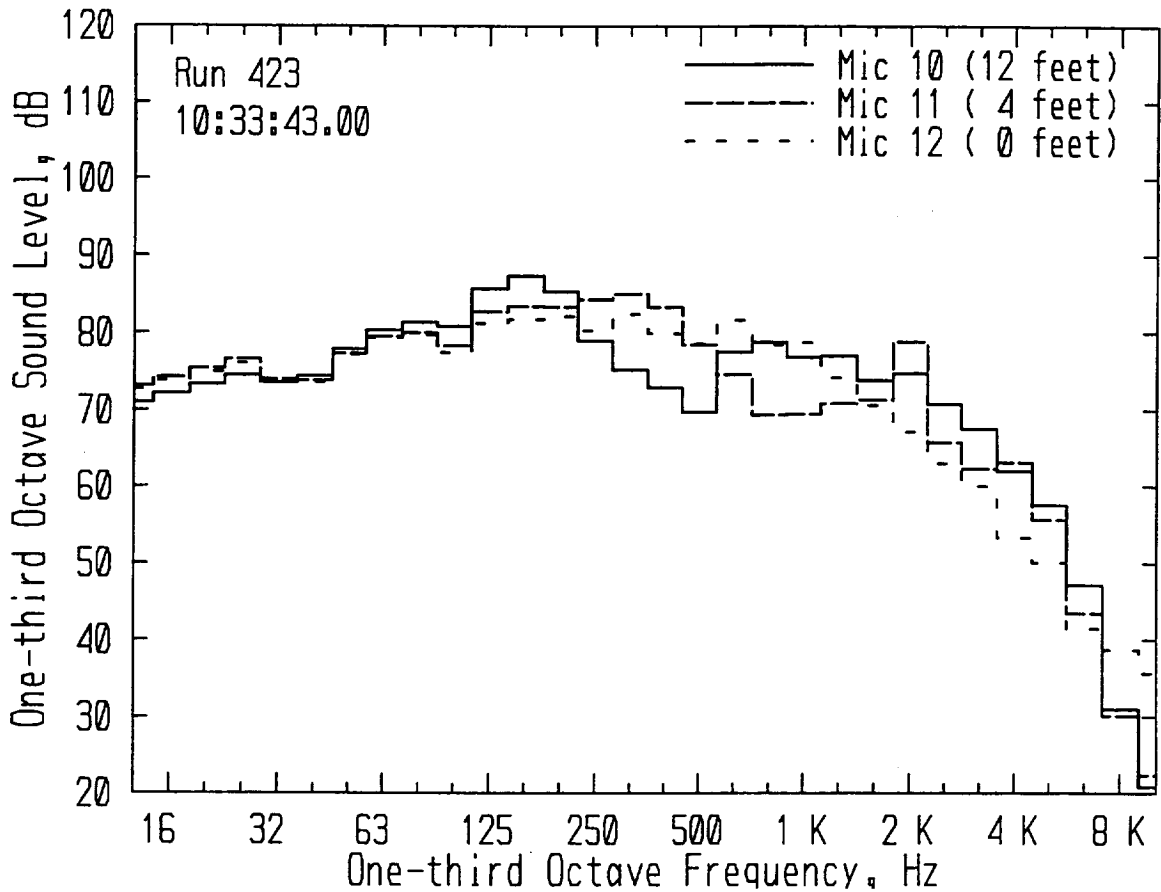
Figure 20. Propagation-adjusted Spectra, Aircraft Height 140 Feet, Distance 2000 Feet

While application of EGA theory generally improves agreement between spectra measured at different heights, the agreement becomes progressively less good at larger distances. This is expected, since at larger distances, variability due to atmospheric effects should be greater. The one-quarter-second averaging time allowed the aircraft to be treated as point sources. Flight distance in that period was typically 70 to 80 feet, reasonably small compared to the closest distance of 500 feet. The small time period is, however, short enough to be a source of variability.

The example results shown in Figures 13 through 20 are typical of comparisons of one-quarter-second third octave spectra for times when the noise source is in line with the array. This is effectively a replication of the kind of point source measurement which has been used to validate ray-tracing ground impedance theory, but conducted under field conditions for a moving aircraft. These results are not as clean as for more ideal experiments, but exhibit the basic features noted: general reduction of differences, and elimination or reduction of interference pattern maxima and minima.

These point source results provide good support for use of EGA theory. Much of aircraft noise analysis is, however, for cumulative metrics such as L_{dn}, so that calculation of SEL is more important than instantaneous level. Figure 21 shows SEL spectra (integrated over the full event) for the same flight as presented in Figure 13. Note that the ground effect interference pattern, prominent in the one-quarter-second spectrum, is seen, although not as pronounced. The presence of this detail has important practical considerations. Because SEL is a composite of geometries over a flight track, ground effect should properly account for the whole track, not just the point of closest approach. Figure 21 suggests that the point of closest approach is the most important part, and that simplification in this regard may be reasonable.
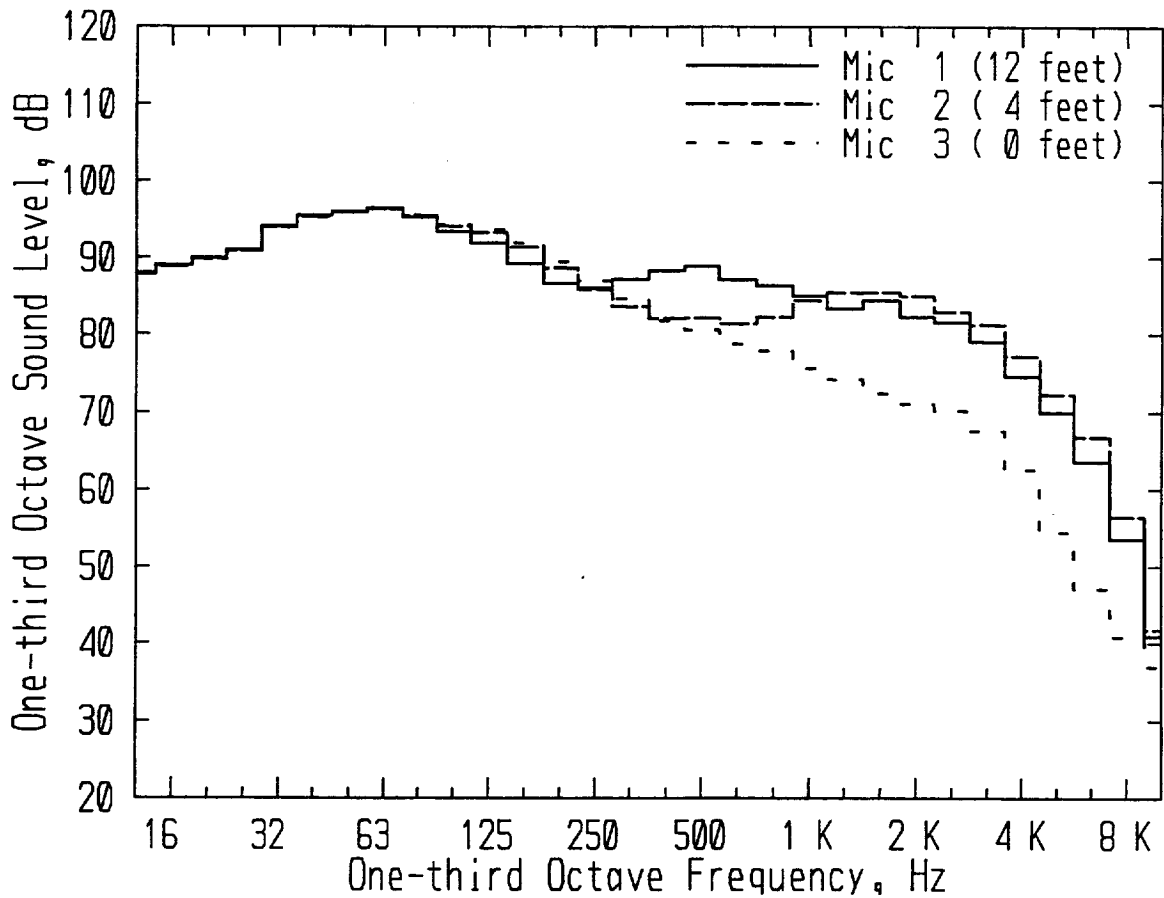
Figure 21. Integrated (SEL) Measured Spectra, Aircraft Height 30 Feet, Distance 666 Feet

5.2 Comparisons of A-Weighted Levels

The results shown in Section 5.1 support the hypothesis that the EGA theory of References 6 and 14-18 is appropriate for aircraft noise modeling. For a wider evaluation, a comparison of A-weighted levels has been made for all of the 162 analyzed flights. The comparison is based on "depropagating" each measured level by adding back in the losses associated with distance, air absorption and ground effect. Air absorption and theoretical ground effect are applied to the measured spectra. The models of References 3 and 4 are also included in the comparison, applied as an A-weighted adjustment.

Because INM and NMAP are line-source models, the comparison would ideally be based on SEL. The measurement site, as described in Section 3.2, is not ideal. The flat area containing the microphones was flat for an extent of about 1000 feet uptrack and downtrack of the microphones. The flight paths were not at constant height: when airborne the aircraft were climbing, and part of each full SEL event included ground roll.

Analysis of A-weighted levels therefore was conducted on a basis similar to that used for spectral analysis: concentration on the region around the point of closest approach. Noise was averaged over a period of one and one-quarter seconds: five of the processed one-quarter-second intervals, centered as described for the point-source spectral analysis in Section 5.1. Calculation of air absorption and theoretical ground effect accounted for the distance and propagation geometry associated with each of the five segments. These were applied to the one-third octave spectral bands, and A-weighted levels computed from the depropagated spectra. Inverse square law was applied so that the final adjusted levels corresponded to a distance of 666 feet, the closest microphone array. The final adjusted levels are denoted "L_{adj}".

As a final normalization, L_{adj} at each microphone was referenced to L_{adj} at microphone 1, which was 12 feet high and 666 feet distant. If propagation effects were perfectly accounted for, $L_{adj} - L_1$ (where L_1 is L_{adj} at microphone 1) would be zero.

Note that this "normalized adjusted level" involves calculation of ground effect for both microphone positions: the one being considered and the reference microphone. If the elevation angle to the reference microphone is high enough that there is little or no ground effect, then the comparison directly evaluates the ground effect model at the microphone being considered. In that case, if this quantity is positive, then measured noise levels are

higher than the model predicts. In this study, elevation angles to the reference microphone are between 3 degrees and 27 degrees, with about half the data being below 10 degrees. Referring to Figure 1, ground effect can be significant for the reference microphone. This means that scatter will be compounded by ground effect being a variable for both microphones. Also, the sign of the difference does not necessarily indicate over or under prediction, but is related to the shape of the ground effect curve. Zero difference still remains an indication of validity of the ground effect model.

The above issues are consequences of performing this analysis among the microphones in the lateral array. The effect of the ground on the reference microphone could be avoided by having a reference microphone on the ground, directly under the aircraft. That was, of course impossible on an active runway, and this method does (as noted earlier) avoid issues of directivity of the aircraft itself. In Section 5.3, this analysis is examined using the end-of-runway measurements as a reference. That alternate analysis avoids the current problem, but includes the question of aircraft lateral directivity and the possibility that aircraft power changed, between the two positions.

Figures 22 through 24 show L_{adj} - L_1 for all microphones and all events, with ground effect adjusted according to SAE 1751, NMAP and impedance theory EGA, respectively. Each figure is plotted as a function of elevation angle, β. The data look substantially the same if plotted as a function of reflection angle φ. A best-fit curve, of the form $ae^{-b\beta}$, is shown on each figure.

All three figures show considerable scatter. For the two empirical models (Figures 22 and 23), the average is well below zero at small angles, while the EGA model has very small difference. The mean results for EGA are gratifying, and suggest that EGA would be more appropriate than either empirical model for long-term averages. The scatter, however, lends an air of uncertainty to any of the models.

The cause of the scatter is refraction by wind and/or temperature gradients. As seen in Figure 1, ground effect is very sensitive to elevation angle β and reflection angle φ. Gradients will cause the sound rays to be curved, rather than straight, affecting both the reflection angle and the phase difference between direct and reflected rays.
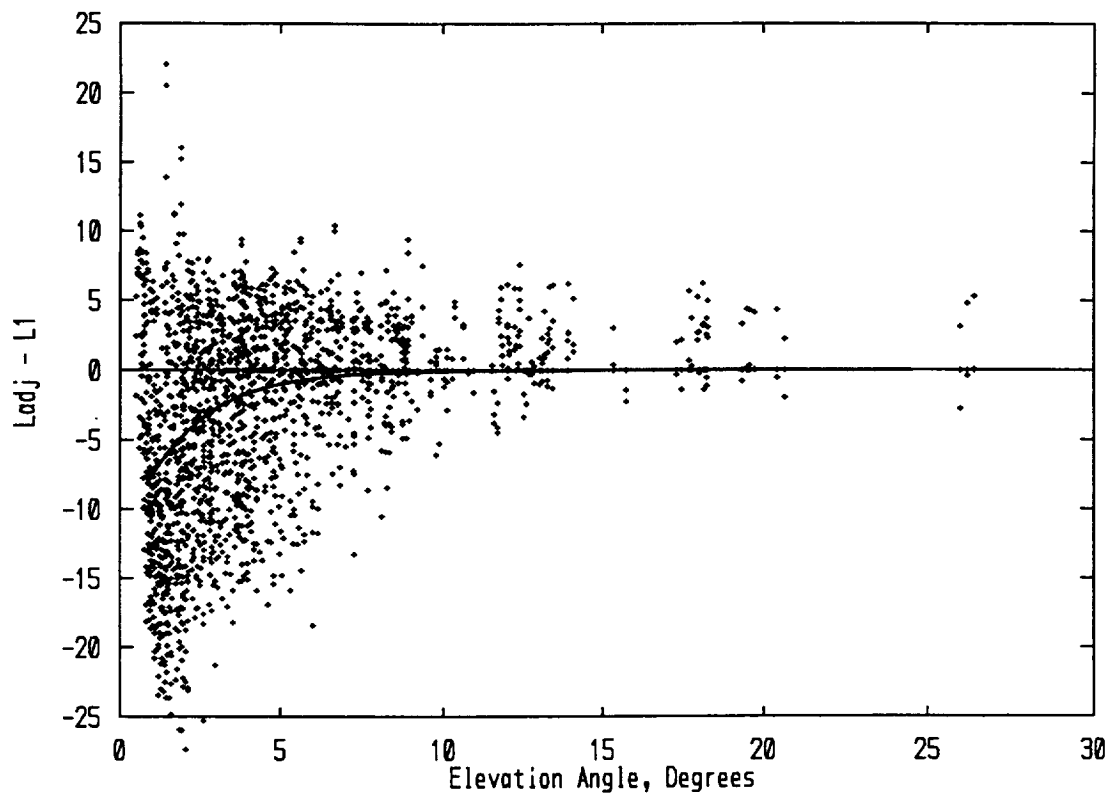
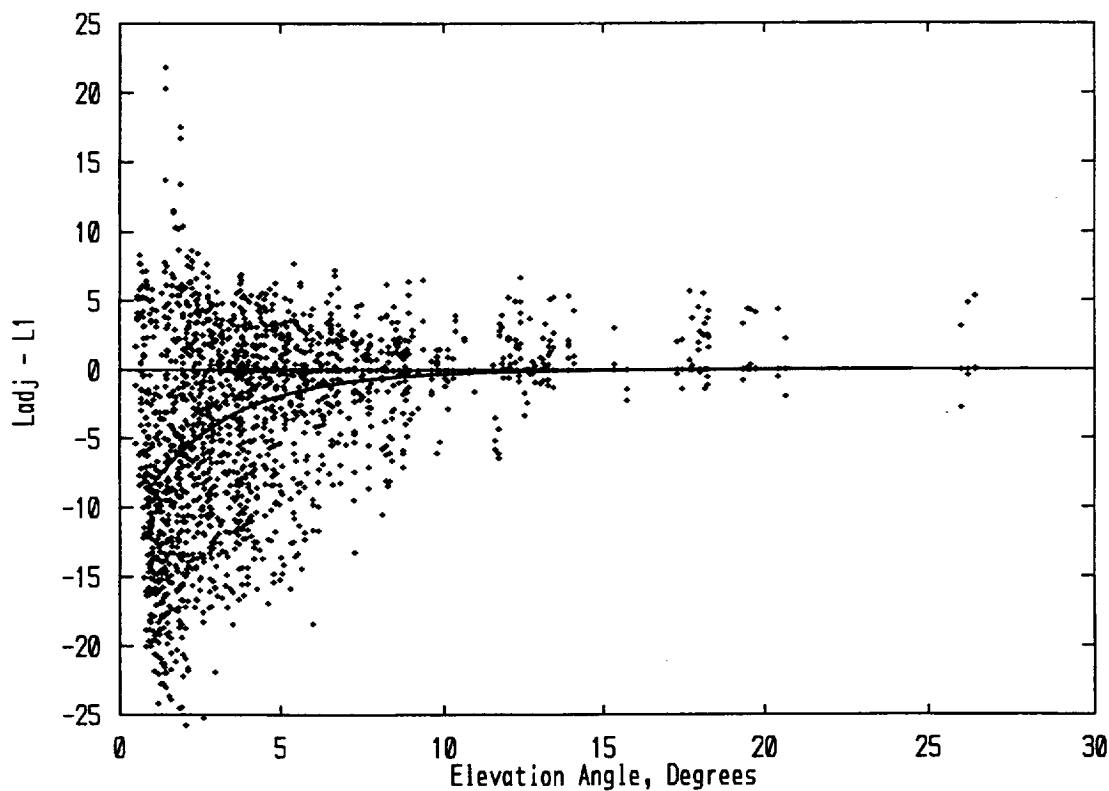**Figure 22. Normalized Noise Levels, Adjusted via SAE Lateral Attenuation Model**

Figure 23. Normalized Noise Levels, Adjusted via NMAP Lateral Attenuation Model
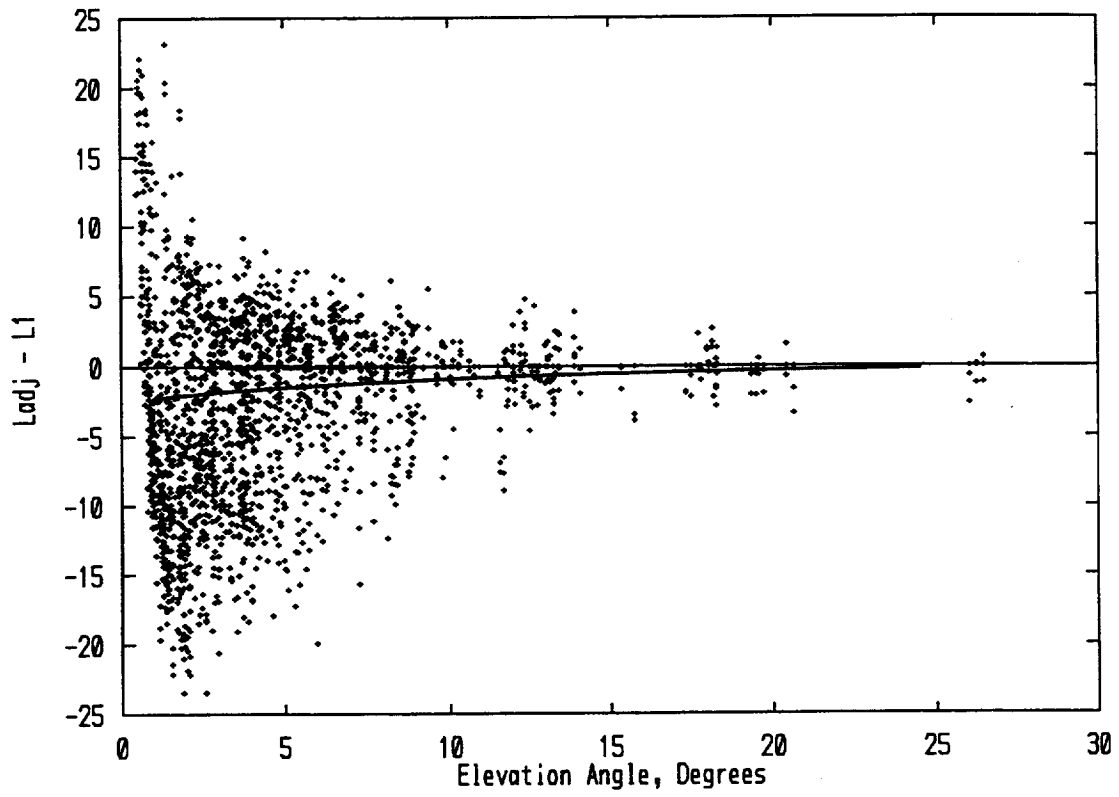
Figure 24. Normalized Noise Levels, Adjusted via EGA Ground Impedance Model

Figures 25 through 27 show the effect of wind. For each event, the component of wind in the direction of propagation was computed, and subsets of data from Figure 24 (normalization by EGA) were analyzed.

Figure 25 shows data for upwind propagation, where rays curve upward and ground attenuation is expected to be stronger than for straight rays. Data in this figure are generally those seen in the lower half of those seen in Figure 25, and the mean curve is negative at small angles, showing that measured levels were lower than predicted.
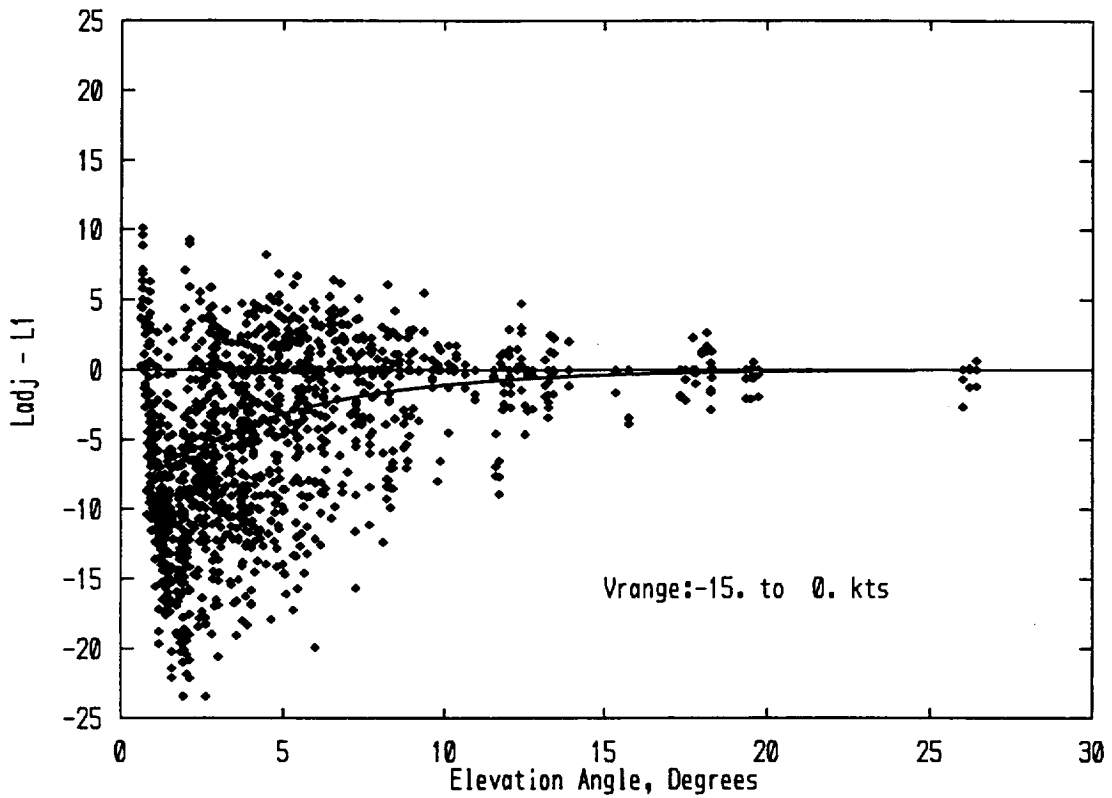
Figure 25. Normalized Noise Levels, Upwind Propagation, EGA Model

Figure 26 shows data for downwind propagation, where rays curve downward and ground attenuation is expected to be less than for straight rays. The mean curve is positive, although the subset is not as distinctly "upper half" as the data in Figure 25 is "lower half". The sign of the wind component may not have been the appropriate demarcation for the two subsets. The normal temperature gradient in the atmosphere is equivalent to upwind propagation of several knots; the empirical models are described as being for "moderate downwind" conditions to compensate for that.
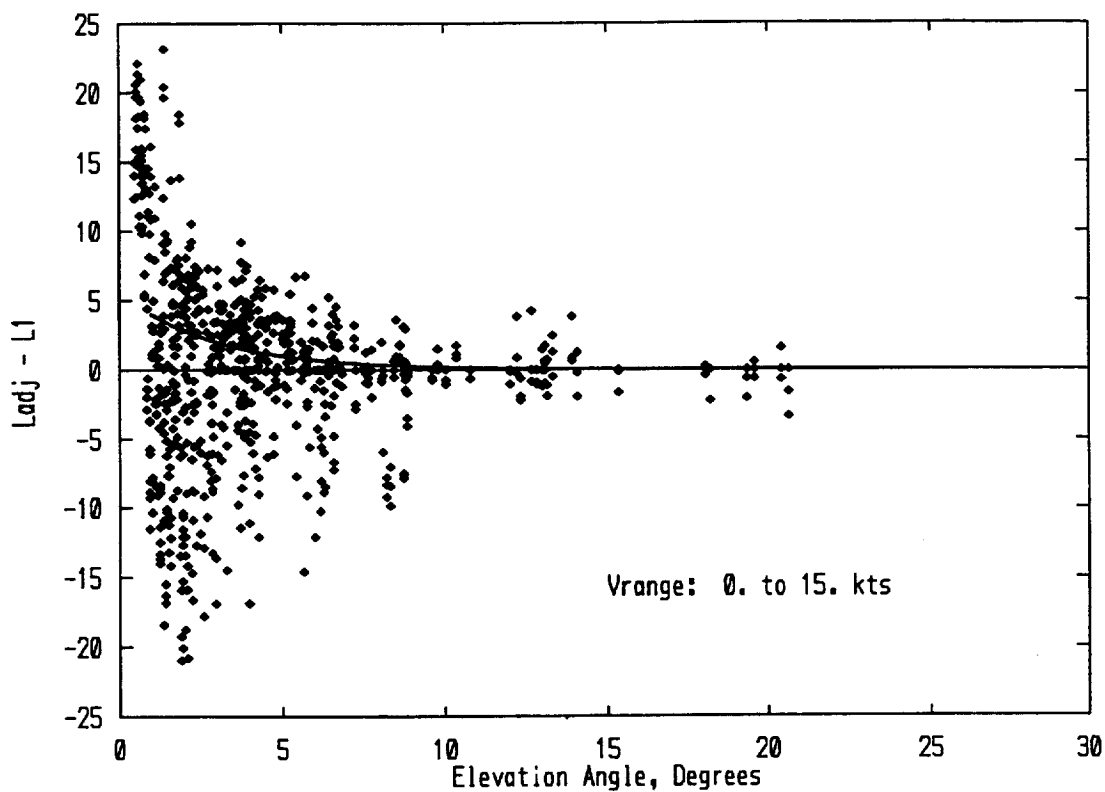
Figure 26. Normalized Noise Levels, Downwind Propagation, EGA Model

The effect of wind is most clearly seen in Figure 27, which shows data for downwind propagation with speeds above 10 knots. In this case, there is virtually no ground attenuation, so the positive curve clearly shows that noise levels are higher than those predicted using EGA. The scatter in the data is also dramatically less than that seen in the other figures.
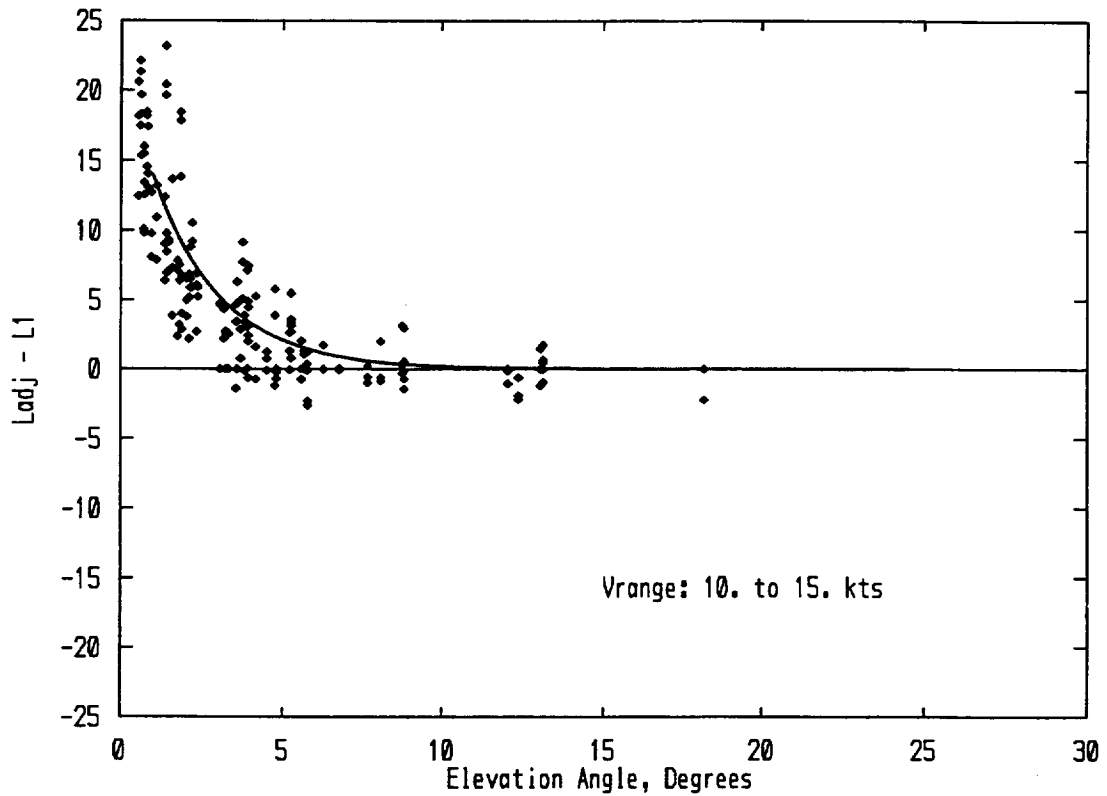

Figure 27. Normalized Noise Levels, Strong Downwind Propagation, EGA Model

The mean "error" seen in Figure 27 corresponds exactly to the application of EGA in a situation where wind obviates it. Figure 28 shows the same strong downwind data set, but without the EGA normalization. The mean is essentially zero. There is still scatter in the data, but this scatter is well within the range occurring in general measurements of aircraft noise, as seen in Reference 18.
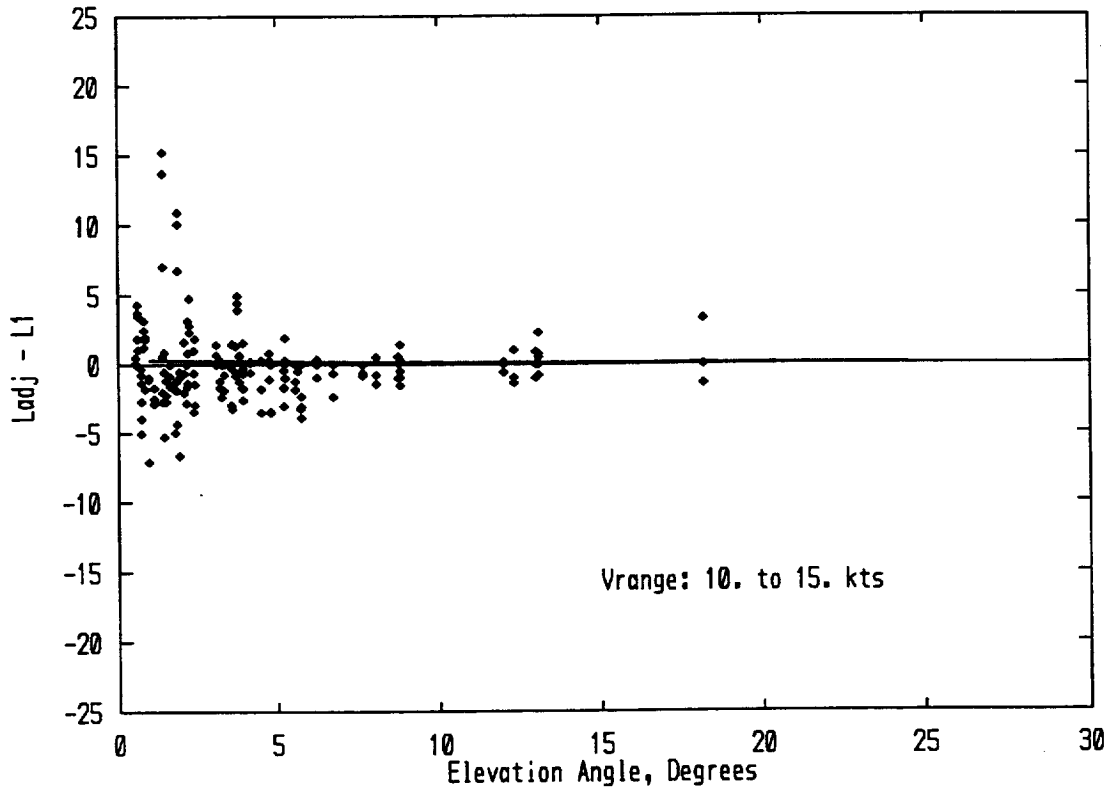

Figure 28. Normalized Noise Levels, Strong Downwind Propagation, No Ground Model

5.3 End-of-Runway Reference

Figure 29 shows the measured noise levels, adjusted via the EGA ground impedance model, referenced to the end-of-runway measurements. Levels from the reference microphone, which was on a hard block on the ground, were adjusted by 6 dB to correspond to the effective free field ground-adjusted lateral array data. Figure 29 is equivalent to Figure 24, with a difference of reference microphone. Because the reference microphone is on a hard ground plane and flights are overhead, the evaluation of ground effect is absolute, rather than relative as for Figure 24 which has a low-angle reference.

Data scatter in Figure 29 is somewhat greater than seen in Figure 24, with more data at points with positive L_{adj} - L_1. Average differences are still positive at high elevation angles, indicating that levels at the lateral array are higher than at the end of runway position.

The assumption in placing the end of runway microphone was that the aircraft's noise emission would be the same there as at the lateral array, and this measurement was made as close as possible to the runway. At Denver, noise abatement cutbacks begin at an altitude of 1000 feet above field level. Review of altitudes at the point of closest approach to the end of runway microphones shows that 2/3 of the aircraft are above 1000 feet, and therefore would have begun their abatement procedures. Examination of some of the time histories show that the maximum levels tend to occur before the point of closest approach, as opposed to occurring after the point of closest approach as was seen at the lateral array. That confirms that cutbacks were occurring at the end of runway position. Lower levels at the reference microphone are consistent with a significant fraction of points in Figure 29 showing positive levels. Because of this, the end of runway reference data are not usable for analysis of the lateral array data.
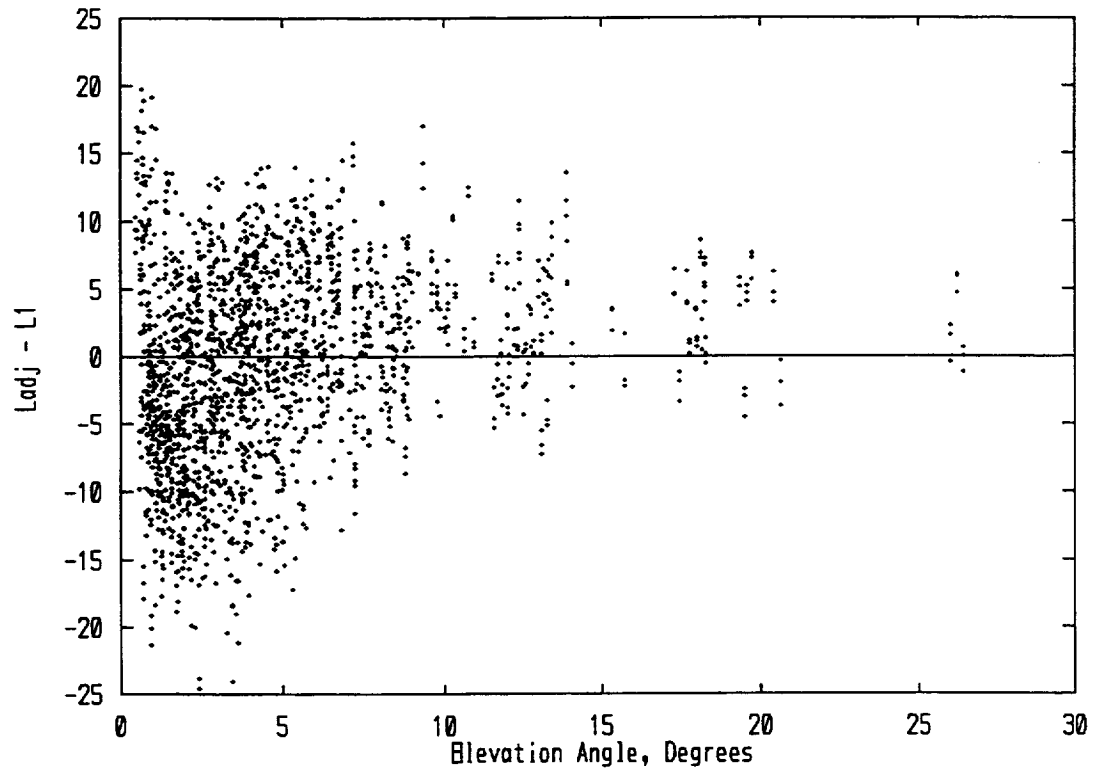
Figure 29. Normalized Noise Levels, Adjusted via EGA Ground Impedance Model, Referenced to End of Runway Measurement

6.0 Conclusions

Measurements have been made of the lateral attenuation of noise from air carrier aircraft in actual operations. Measurements were directed toward ground propagation effects, and included distances up to 2000 feet from the runway centerline and elevation angles up to 27 degrees.

Lateral attenuation models currently used in the INM and Noisemap computer programs tended to overpredict attenuation, i.e., noise levels predicted by these models would tend to be lower than measured. Lateral attenuation computed from modern ground impedance theory agrees well with average measured attenuation.

Differences between the models occur at small elevation angles. Above about 5 degrees, average ground attenuation is not a major factor.

There is large variability between measured and predicted lateral attenuation at small angles. This is because sensitivity to actual ray path lengths and reflection angles, both of which can be influenced by wind and temperature gradients. Wind conditions can significantly alter these parameters. Substantial variations in levels for single events can occur at nominal elevation angles up to 10 to 15 degrees.

Because of the improved average performance of the ground impedance theory, consideration should be given to updating INM and Noisemap to use algorithms based on this theory.

References

1. Integrated Noise Model (INM) Version 5.0 User's Guide, FAA-AEE-95-01, August 1995.

2. Czech, J.J., and Plotkin, K.J., "NMAP 7.0 User's manual", Wyle Research Report WR 98-13, November 1998.

3. "Prediction Method for Lateral Attenuation of Airplane Noise During Takeoff and Landing", Standards, SAE AIR 1751, Society of Automotive Engineers, Warrandale, PA (1981).

4. Speakman, J.D. and Berry, B.F., "Modeling Lateral Attenuation of Aircraft Flight Noise", *Proceedings of Inter-Noise 92*, Toronto, Canada, July, 1992 pp 877-882.

5. Plovsing, B. "Aircraft Sound propagation over Non-Flat Terrain. Development of Prediction Algorithms", AV 1015/93, DELTA Acoustics & Vibration, Danish Acoustical Institute (1994).

6. Chien, C.F., and Soroka, W.W., J., "A Note on the Calculation of Sound propagation Along an Impedance Surface", J. Sound Vib **69**, 340-343 (1980).

7. Plotkin, K.J., "A Model for the Prediction of Highway Noise and The Effect of Regulations", Wyle Research Report WR74-5, 1975.

8. "Procedure for the Calculation of Airplane Noise in the Vicinity of Airports", SAE Aerospace Information Report AIR 1845, March 1986.

9. Parkin, P.H., and Scholes, W.E., "The Horizontal Propagation of Sound form a Jet Engine Close to the Ground, at Radlett", *J. Sound and Vibration* **1**, 1-13, (1964).

10. Parkin, P.H., and Scholes, W.E., "The Horizontal Propagation of Sound form a Jet Engine Close to the Ground, at Hatfield", *J. Sound and Vibration* **2**(4), 353-374, (1965).

11. Fleming, G.G., Olmstead, J.R., D'Aprile, J.R., Gerbi, P.J., Gulding, J.M., and Plante, J.A., "Integrated Noise Model (INM) Version 5.1 Technical Manual", Report No. FAA-AEE-97-04, December 1997.

12. Speakman, J.D., "Lateral Attenuation of Military Aircraft Flight Noise", AAMRL-TR-89-034, July 1989.

13. Moulton, C.L., "Air Force Procedure for Predicting Noise Around Airbases: Noise Exposure Model (NOISEMAP) Technical Report", Wyle Research Report WR 91-2 (also AL-TR-1992-0059) (1992).

14. Embleton, T.F.W., Piercy, J.E., and Olson, N., "Outdoor Sound Propagation Over Ground of Finite Impedance", *J. Acoust. Soc. Am*, **59**, 267-277 (1976).

15. Embleton, T.F.W, "Tutorial on Sound Propagation Outdoors", *J. Acoust. Soc. Am.*, **100** (1), 31-48, July 1976.

16. Chessell, C.I., "Propagation of Noise Along a Finite Impedance Boundary", *J. Acoust. Soc. Am*, **62**, 825-834 (1977).

17. Delaney, M.E., and Bazley, E.N., "Acoustical Properties of Fibrous Absorptive Materials", *Appl. Acoust.* **3**, 105-116 (1970).

18. Page, Juliet A., Hobbs, Christopher M., and Stusnick, E., "Validation of Aircraft Noise Prediction Models at Low Levels of Exposure Phase 2 - Final Report Volume I - Low Level Measurements", Wyle Research Report WR98-11, February 1999.

REPORT DOCUMENTATION PAGE

1. AGENCY USE ONLY (Leave blank)	2. REPORT DATE April 2000	3. REPORT TYPE AND DATES COVERED Contractor Report

4. TITLE AND SUBTITLE
Examination of the Lateral Attenuation of Aircraft Noise

6. AUTHOR(S)
Kenneth J. Plotkin, Christopher M. Hobbs, and Kevin A. Bradley

5. FUNDING NUMBERS
C NAS1-20103, Task 22

WU 538-03-15-01

7. PERFORMING ORGANIZATION NAME(S) AND ADDRESS(ES)

The Boeing Company
2401 East Wardlow Road
Long Beach, CA 90807-4418

Wyle Laboratories (Subcontractor)
2001 Jefferson Davis Highway
Arlington, VA 22202

8. PERFORMING ORGANIZATION REPORT NUMBER

9. SPONSORING/MONITORING AGENCY NAME(S) AND ADDRESS(ES)

National Aeronautics and Space Administration
Langley Research Center
Hampton, VA 23681-2199

10. SPONSORING/MONITORING AGENCY REPORT NUMBER

NASA/CR-2000-210111

11. SUPPLEMENTARY NOTES
Langley Technical Monitor: Kevin P. Shepherd

12a. DISTRIBUTION/AVAILABILITY STATEMENT

Unclassified-Unlimited
Subject Category 71   Distribution: Nonstandard
Availability: NASA CASI (301) 621-0390

12b. DISTRIBUTION CODE

13. ABSTRACT (Maximum 200 words)
Measurements of the lateral attenuation of noise from aircraft operations at Denver International Airport were made at distances up to 2000 feet and elevation angles up to 27 degrees. Attenuation calculated from modern ground impedance theory agrees well with average measured attenuation. The large variability between measured and predicted levels observed at small elevation angles is demonstrated to be due to refraction by wind and temperature gradients.

14. SUBJECT TERMS

Noise - Aircraft Noise Prediction

15. NUMBER OF PAGES
61

16. PRICE CODE
A04

17. SECURITY CLASSIFICATION OF REPORT Unclassified	18. SECURITY CLASSIFICATION OF THIS PAGE Unclassified	19. SECURITY CLASSIFICATION OF ABSTRACT Unclassified	20. LIMITATION OF ABSTRACT UL